Lawrence Berkeley National Laboratory
Lawrence Berkeley National Laboratory

Title
TEMPERATURE MEASUREMENTS IN THE TORMAC IV-c PLASMA

Permalink
https://escholarship.org/uc/item/4z75466g

Author
Greenwald, Martin

Publication Date
1978-09-01

eScholarship.org Powered by the California Digital Library
University of California

RECEIVED BY TIC FEB 12 1979

LBL-8166

MASTER

# TEMPERATURE MEASUREMENTS IN THE TORMAC IV-c PLASMA

Martin Greenwald
(Ph. D. thesis)

September 1978

Prepared for the U. S. Department of Energy
under Contract W-7405-ENG-48

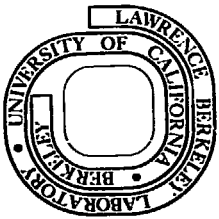

Martin Greenwald

Lawrence Berkeley Laboratory
University of California
Berkeley, California 94720

## TABLE OF CONTENTS

# Temperature Measurements in the Tormac IV-c Plasma*

Martin Greenwald

Accelerator and Fusion Research Division
Lawrence Berkeley Laboratory
University of California
Berkeley, California 94804

## ABSTRACT

A magnetic confinement device TORMAC IV-c, was built to test the Tormac concept and the results of TORMAC IV-a. The new device had improved access for diagnostics, particularly for laser scattering and He-Ne interferometery. The results were dissappointing; measured electron temperatures were consistently in the range of 5 eV. Peak densities were $5 \times 10^{15}/cm^3$. Under these highly collisional conditions, no conclusions about Tormac confinement could be drawn.

Tormac, an acronym for toroidal magnetic cusp, is part of the controlled fusion effort. It is an attempt to combine the favorable MHD stability properties of an open field line geometry with the good particle confinement inherent in devices with closed toroidal feld lines. The goal is to confine a high beta plasma with a loss rate that is acceptable for fusion applications.

*Work supported by the U. S. Department of Energy.

## INTRODUCTION

This thesis is divided into four main parts. The first is an introduction to the Tormac concept and a brief summary of the theoretical problems involved. The second part describes the experimental work with little detail. Both the construction and diagnostics are summarized. The third section is broken into two parts, a summary of the data taken on TORMAC IV-c and an explanation and discussion of the data. Finally, a number of lengthy appendices are included. These detail the construction and operation of the device and describe the principles and practice of the diagnostics employed.

The work of constructing and diagnosing TORMAC IV-c was shared with J. Coonrod, another graduate student. The author was responsible particularly for the Thomson scattering experiment, J. Coonrod for the interferometer and electrical measurements but the work was in general a cooperative effort. The experiment was built to duplicate, as closely as possible, TORMAC IV-a, constructed by Levine and Gallagher at AFCRL with work continued at LBL by Levine and Myers. A good deal of the ancillary hardware on TORMAC IV-c came from the earlier machine.

TORMAC CONCEPT

To be useful for controlled fusion, magnetic confinement schemes must meet both technical and economic requirements. These requirements are at times in conflict; for example confinement times generally increase with increasing reactor size, while economic desirability decreases after some point. High plasma beta is desirable ($\beta = 8\pi p/B^2$) since for a given fusion power output lower magnetic fields can be used. Formation and containment of high beta plasmas are difficult.

Tormac is an attempt to contain high pressure plasmas by combining the stability properties of open field line configurations and the good tranport properties inherent in configurations with closed toroidal fields.

In toroidal systems average minimum B stabilization is not adequate to contain plasmas above certain critical betas.[1] This value depends in detail on the configuration but is typically a few percent. Above this value serious MHD instabilities set in.

Absolute minimum B devices are stable to MHD modes even at very high betas.[2,3,4] However, it can be shown that such configurations require open field lines and they tend to be ineffective in containing particles.[5,6,7] For example (see Figure 1) simple cusps have a central region of low fields. Particles traverse this region in essentially straight line orbits, adiabaticity is not preserved. Particles whose orbits carry them toward the cusp points are lost. The rate of

particle loss is

$$\dot{N} = -n_i v_i \delta \qquad \delta = \text{effective hole size usually taken to be } r_i$$
$$= -n_i v_i r_i$$

The total number of particles is

$$N = n_i r_p^2 \qquad r_p = \text{plasma radius}$$

$$\tau_{cusp} = \frac{-N}{\dot{N}} = \frac{n r_p^2}{n v_i r_i}$$

$$\tau_{cusp} = \frac{r_p^2}{v_i r_i} = \tau_{transit} \frac{r_p}{r_i} = \frac{eB}{kT_i} r_p^2 \text{ ("Bohm" like)}$$

This scaling law is unacceptable for controlled fusion applications.

New theories for cusp confinement show that under some circumstances particles can be held in cusp geometries for times of the order $\tau_{ii}$ (the ion-ion scattering time) similar to confinment in magnetic mirrors.[8,9]

A schematic of the Tormac geometry is seen in Figure 2. The plasma is divided into two regions. An outer region, a thin sheath consists of particles on open field lines. These particles are held for a time $\tau_{ii}$ and have a loss cone distribution analogous to that of a mirror machine. The plasma pressure is maintained across this sheath supported by the open field lines in a minimum B configuration. Particles in the inner region are on closed toroidal field lines. Their velocity distribution is maxwellian. There is little if any

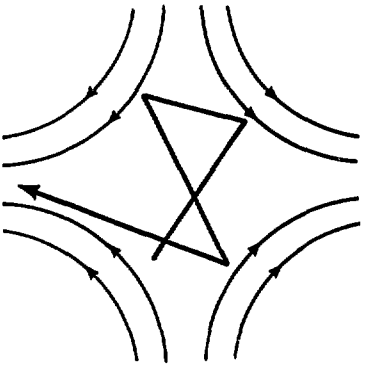

$$\dot{N} = -n_i v_i \delta$$

$$= -n_i v_i r_i$$

$$N = n_i r_p^2$$

$$\tau = \frac{-N}{\dot{N}} = \frac{r_p^2}{v_i r_i}$$

# Particle loss in cusp fields

XBL 789-2202

PARTICLES ARE LOST AT THEIR THERMAL VELOCITIES THROUGH A HOLE OF SIZE $\delta$ TAKEN TO BE AN ION GYRORADIUS IN THIS CALCULATION.

Fig. 1

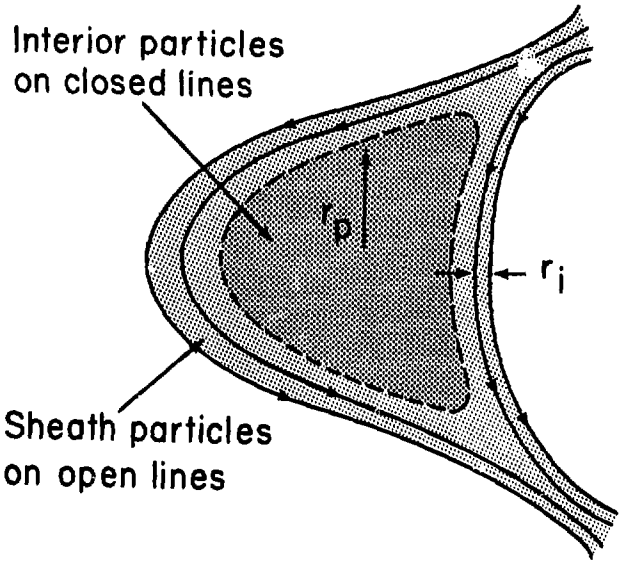


Tormac confinement

XBL 789-2224

Fig. 2

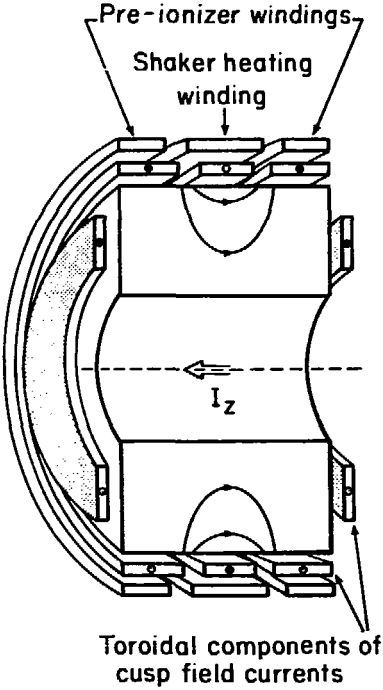


Tormac IV geometry

XBL 789-2223

SCHEMATIC OF TORMAC IV SHOWING THE PLACEMENT OF THE WINDINGS AND THE GLASS VESSEL. THE TOROIDAL AND POLOIDAL CURRENTS ARE SHOWN SEPARATED FOR CLARITY. IN THE ACTUAL EXPERIMENT, BOTH COMPONENTS OF THE CUSP FIELD ARE CREATED BY A SINGLE WINDING.

Fig. 2a

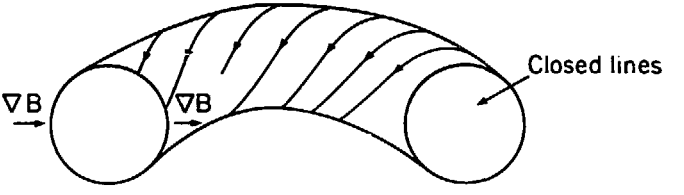


Tokamak average minimum-B geometry

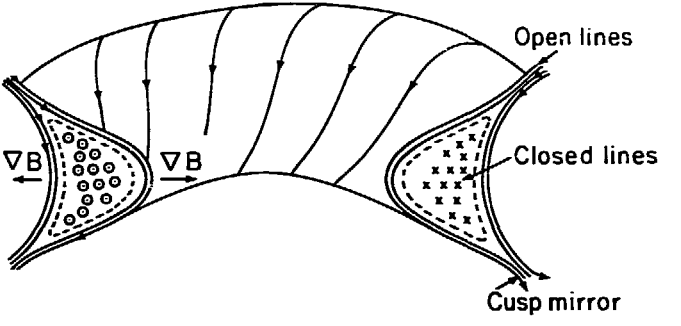


Tormac absolute minimum-B geometry

XBL 789-2222

SCHEMATIC OF THE TORMAC ABSOLUTE MINIMUM B CONFIGURATION CONTRASTED WITH THE TOKAMAK AVERAGE MINIMUM B. IN BOTH CASES, TOROIDAL FIELDS WITH A 1/R DEPENDENCE PROVIDE FAVORABLE CURVATURE AT SMALL MAJOR RADIUS.

Fig. 3

pressure gradient across this portion of the plasma. The inner particles provide a reservoir to resupply the sheath. Overall confinement is thus enhanced over that of a mirror by a geometrical factor $r_p/r_s$, the ratio of plasma to sheath volume.[10]

$$\tau_{tormac} = \frac{r_p}{r_i} \tau_{ii}$$

Sheath thickness is an important parameter in the Tormac scheme. In steady state, particles diffusing into the sheath are balanced by those lost through the cusp. Theoretical studies have shown that sheaths thinner than an ion gyroradius are unstable.[17] Some experiments have shown sheaths with widths of one or two ion gyroradii under conditions similar to those expected in Tormac.[11-15]
With a sheath thickness of an ion gyroradius, Tormac confinement becomes

$$\tau_{tormac} = \frac{r_p}{r_i} \tau_{ii}$$

compared to

$$\tau_{mirror} = \tau_{ii}$$

$$\tau_{cusp} = \frac{r_p}{r_i} \cdot \frac{r_p}{v_i}$$

Confinement is improved over mirror times by the ratio of plasma size to gyroradius, which can be made quite large. Confinement is improved over that of a cusp by $\lambda_i/r_p$, where

$\lambda_i$ is the ion mean free path. In the collisionless regime this can also be a large number.

There are a number of important requirements on the plasma in order to sustain this scenario.

1. Thin, stable sheath
2. Inner region should not mix with sheath
3. Proper startup

The sheath must be stable in the presence of a large $\nabla p$, a loss cone distribution, $p_\perp \neq p_\parallel$ and a drift velocity $v_D \sim v_i$. The last is not obvious but can be shown since

$$\frac{\bar{J}}{c} \times \bar{B} = \bar{\nabla} \bar{p}$$

$$J = ckT \frac{\nabla n}{B} \qquad \text{(assume isothermal with } T_e \sim T_i\text{)}$$

also $J = nev_D$

so $v_D = \frac{\nabla n}{n} \frac{mv_i^2 c}{eB} = v_i \frac{r_i}{\delta}$

for $\delta \approx r_i$, $v_o \approx v_i$

(note for $\delta < r_i$, $v_D > v_i$ probably unstable)

The concern here is for microinstabilities which could lead to enhanced diffusion thus an increase in $\delta$ and very likely enhanced particle loss. A number of these have been studied; results so far look promising, largely due to the stabilizing influence of higher beta (for microinstabilities) and the presence of highly sheared fields in the sheath.[16-22]

If particles from the inner region mix with sheath

particles, the loss cone distribution would be rapidly communicated and the containment time drastically shortened. To prevent this occurrence, the drift orbits of the inner particles must be closed up. A rotational transform can accomplish this (Figure 4). It need not be large, in the vacuum field

$$v_D = \frac{v_\perp^2}{\Omega_i R}$$

$\Omega_i$ = ion cyclotron frequency

R = major radius

the drift across the minor radius is in a time

$$\Delta t_D = \frac{r_p}{v_D} = r_p R \Omega_i / v_\perp^2$$

We need a rotational transform large enough to move the particles back. They will circulate at a frequency

$$\omega_R = \frac{2 v_\parallel \iota}{R} \qquad \iota = \text{rotational transform}$$

$$\Delta t_R = \frac{R}{2 v_\parallel \iota}$$

equating these times $\frac{r R \Omega_i}{v_\perp^2} = \frac{R}{2 v_\parallel \iota}$

thus we need

$$\iota = \frac{r_i}{2 r_p}$$

but

$$\iota \equiv \frac{B_p}{B_T} \frac{R}{r}$$

so $B_p = B_T \left(\frac{r}{R}\right)\left(\frac{r_i}{2r_p}\right) \sim B_T \left(\frac{1}{4}\right)\left(\frac{1}{20}\right)$

where the aspect ratio has been taken to be 4 and the ratio

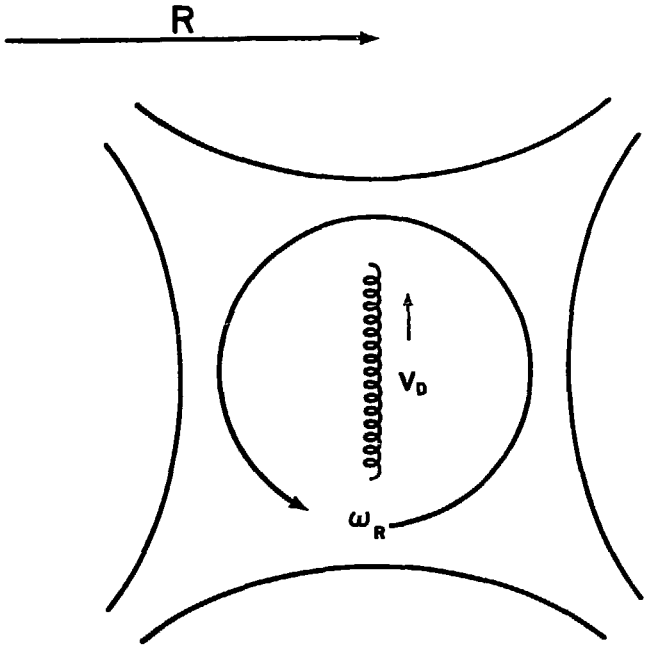


Geometry for drift orbit calculation

XBL 789-2206

$V_D$ IS THE DRIFT VELOCITY IN THE NONUNIFORM INTERNAL TOROIDAL FIELD. $\omega_R$ IS THE CIRCULATION FREQUENCY AND IS DETERMINED BY THE ROTATIONAL TRANSFORM AND THE PARALLEL VELOCITY OF THE PLASMA PARTICLES.

Fig. 4

of plasma radius to sheath size set equal to 10.

Even if the Tormac configuration can be shown to be a stable equilibrium with the transport properties described above, we are still faced with the problem of creating it. The problem is formidable. The present method, creating a diffuse toroidal "z" pinch on which the cusp field is superimposed, demonstrates some of these difficulties. The pinch is unstable and would be quickly destroyed if it were very hot. A cold plasma target must be heated before particle and energy losses and field diffusion destroy the configuration. Open field lines can bring the plasma into contact with the walls and cool it quickly through parallel conduction. Cold plasma and neutrals can lead to large perpendicular losses. If field diffusion in the cold plasma is rapid, the field free region might be small or nonexistent by the time the plasma has been heated.

THE BICUSP[23]

Tormac IV is a bicusp configuration. Figure 2a shows the basic arrangement of coils and plasma. Figures 5a and b are detailed plots of the actual fields. The bicusp has an advantage over higher order multipoles in that all cusps are at the same major radius. This has been shown to decrease the size of the sheath loss cone.[24] At first glance it would not appear to be a minimum B geometry, since the curvature of the poloidal fields is unfavorable for small major radius.

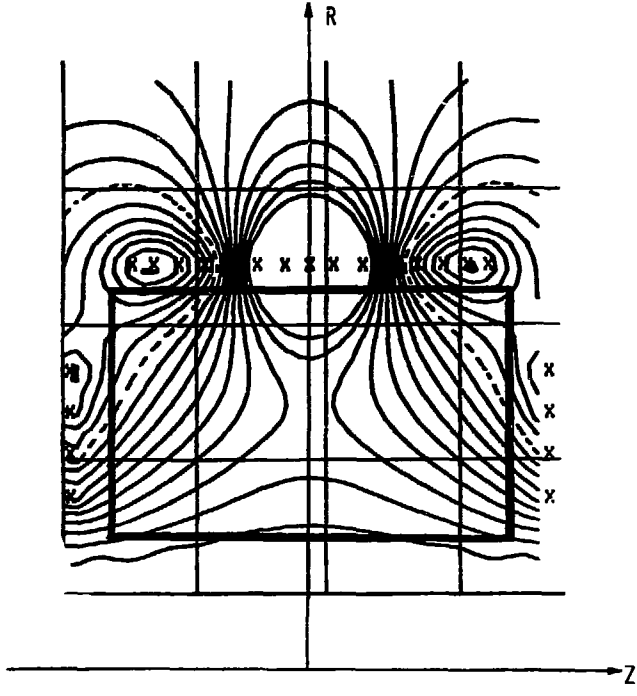


POLOIDAL FIELD LINES (PSI CONTOURS) OUTPUT FROM VACUUM FIELD PROGRAM. THE POSITION OF THE GLASS VESSEL IS SHOWN BY HEAVY LINES.

XBL 789-11085

Fig. 5a

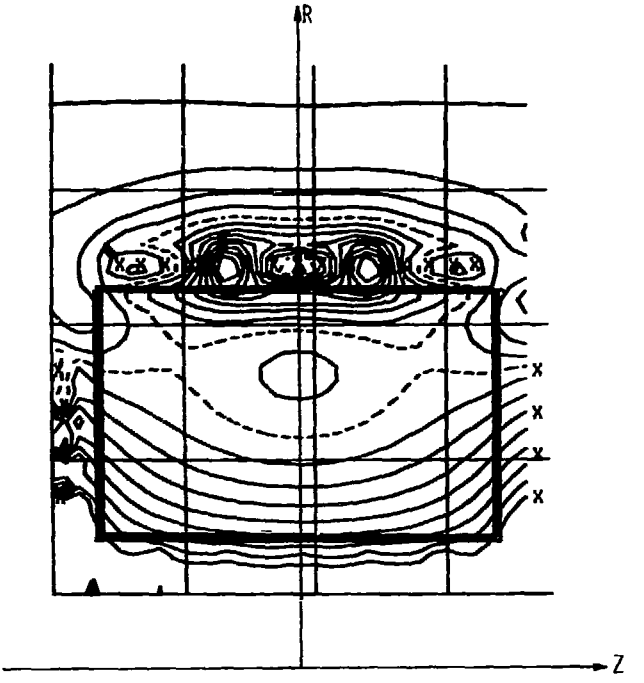


|B| CONTOURS, OUTPUT FROM VACUUM FIELD PROGRAM. THE POSITION OF THE GLASS VESSEL IS SHOWN BY HEAVY LINES.

XBL 789-11084

Fig. 5b

However, the toroidal field dominates in this region, giving favorable curvature everywhere. This is confirmed by the $|B|$ plots.

TORMAC IV-c

In order to test the Tormac principle and to investigate the "shaker" heating technique, TORMAC IV (the fourth in a series of Tormac experiments) was built at Air Force Cambridge Research Laboratories.[25,26] This experiment was later moved to the Lawrence Berkeley Lab and began operation at the beginning of 1975.[27,28] From spectral and electrical diagnostics, ion temperatures of 100 to 300 eV and densities of several times $10^{15}$, lasting for 50 to 100 microseconds were inferred. These measurements, if correct, would be significant.

To test these results TORMAC IV-c was built as a close duplicate to IV-a. It had greatly improved diagnostic access permitting measurement of electron temperature by 90° Thomson scattering, electron density by the He-Ne interferometry, and field and current measurements, using magnetic probes. The new vacuum vessel and windings matched, as closely as possible, the old configuration. It uses the old capacitor banks and vacuum pumps but has a larger vacuum manifold for faster pumping. The main cusp windings are more strongly reinforced, allowing operation at higher fields if this proved desirable.

EXPERIMENTAL DETAILS

The vacuum vessel, made of pyrex, is toroidal with a

rectangular cross section 24 x 14 cm (see figure 6). Its major radius (to the outer circumference) is 22 cm. A turbo molecular pump is used and base pressure in the vessel is $6 \times 10^{-7}$ torr. A pneumatically operated gate valve isolates the pump from the vessel during a run. A set of solenoid valves allows for automatic gas filling.

The main cusp windings consist of 100 parallel wires wrapped in a solenoid of varying pitch, creating both poloidal and toroidal fields. Current is returned through the center of the torus by a 5" diameter copper pipe. Details are shown in figure 7. The main coil is powered by a 113 μF capacitor bank charged ordinarily to 15 kV. At this voltage it contains 12.8 kJ. The bank is connected to a passive crowbar with 16 low inductance cables and to the experiment via an 8" wide stripline. The system has a measured risetime (T/4) of 8.3 microseconds, implying an inductance of 250 nH. Peak current at 15 kV charging is 268 kA, providing a 4.5 kG field at the plasma surface. The crowbarred current decays with a 1/e time of 80 microseconds. This can be extended if plasma behavior requires it. Ignitrons provide series and crowbar switching (see Figure 8).

A pair of toroidal straps, wired in parallel, serve for preionizing the plasma. They are powered by a 2 μF capacitor charged to 30 kV, for an energy of 900 J. The circuit rings at 110 kHz setting up a large electric field and driving a toroidal current (approximately 40 kA peak). The preionizer

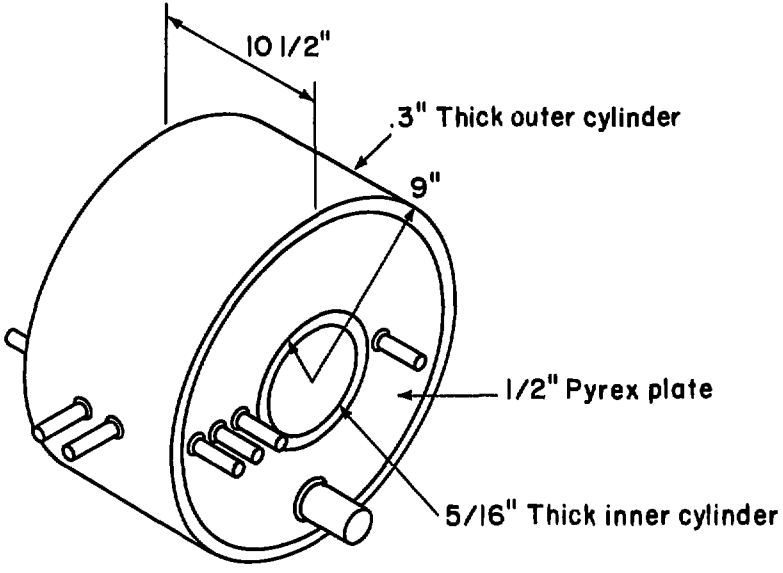


**Glass vessel and access**

XBL 789-2219

Fig. 6a

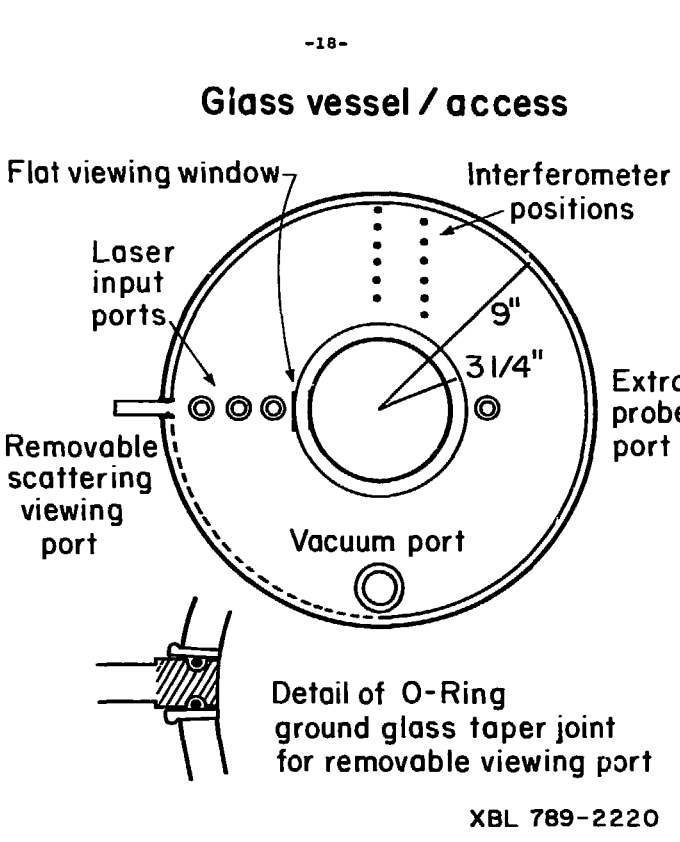
Glass vessel / access
Flat viewing window
Interferometer positions
Laser input ports
9"
31/4"
Extra probe port
Removable scattering viewing port
Vacuum port
Detail of O-Ring ground glass taper joint for removable viewing port
XBL 789-2220

Fig. 6b

Coil assembly

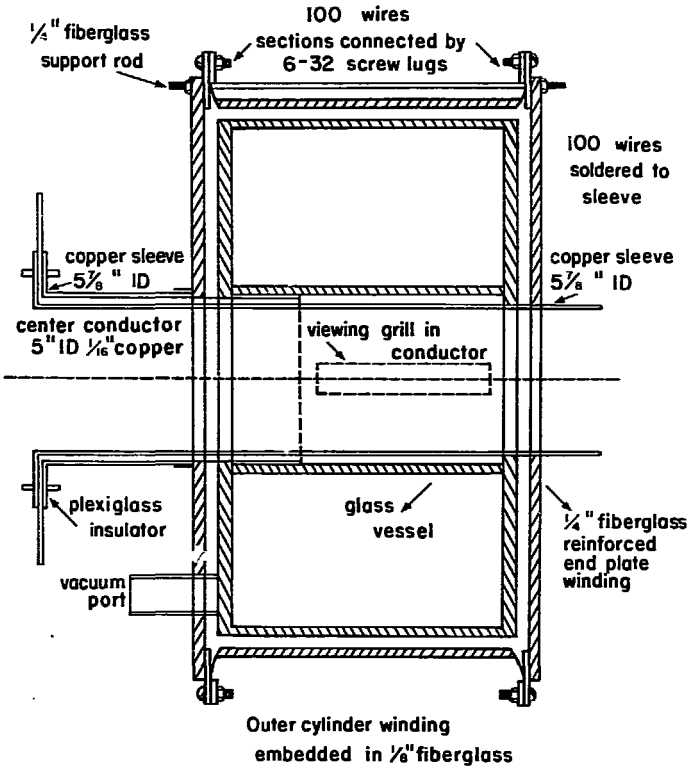


Fig. 7

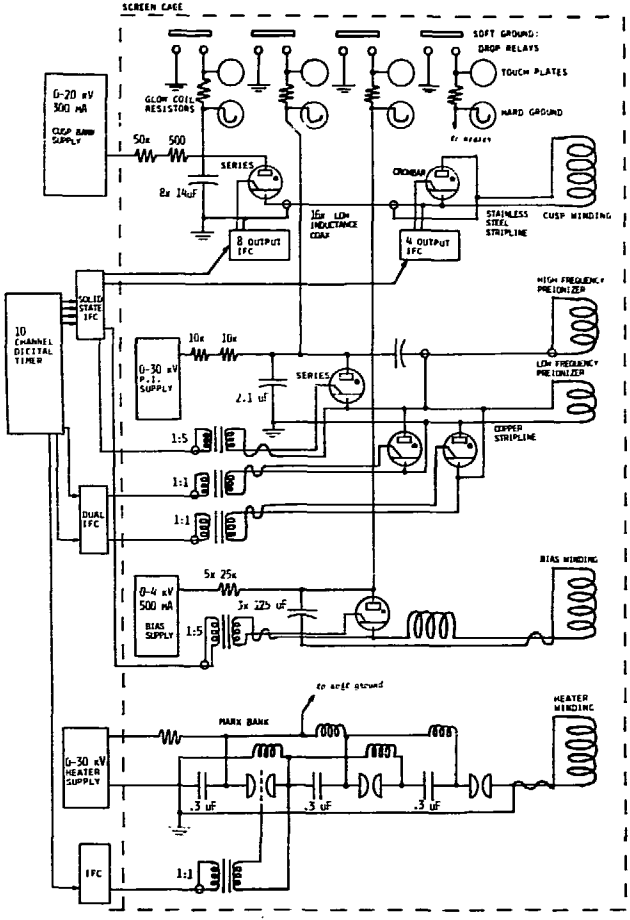


Fig. 8

XBL 789-10873

can be crowbarred during any phase of its oscillation. A smaller low capacitance bank, powered by the larger one, drives a high frequency current in two additional loops and aids in initial gas breakdown.

Toroidal bias field (which will become the stuffing field in the compressed plasma) is applied from a loosely wound, eight turn solenoid. A 375 μF capacitor charged to 2 kV drives a 300 G field which rises in about 200 microseconds.

The first operation in the firing sequence involves closing the gate valve and filling the vessel with 10 to 100 mTorr of gas (85% $D_2$, 15% He). The bias field is turned on, and when it reaches its peak, the gas is broken down by the ionizer. After 15 or 20 microseconds ionization has reached its peak and the bank is crowbarred; the bias field should be frozen in by the conductive plasma. The cusp bank is fired, reaching a peak in 8.3 microseconds. The cusp bank is crowbarred and the fields and plasma decay away. A ten channel digital delay unit provides the timing for the sequence. Delays are adjustable from .1 to 1000 microseconds with .1 microsecond resolution and accuracy.

## DIAGNOSTICS

Diagnostics on TORMAC IV-c fall into two general categories, optical and electrical. The optical diagnostics include Thomson scattering, He-Ne interferometry, and spectroscopy. electrical diagnostics were Rogowski belts, a flux loop, and

magnetic probes.

The Thomson scattering system is discussed in detail in appendix B. To summarize, it consists of the following parts: a ruby laser, Q switched, delivering 2 to 4 joules at 6943 A in 25 nanoseconds; input optics, lenses, apertures, and mirrors to clean up the beam, focus it and steer it through the vessel; a beam dump of CS 4-72 glass set at the Brewster angle; viewing optics, lenses and mirrors to image scattered light into the polychromator; a polychromator, a triple grating configuration, designed to reject strong light at 6943 A; photomultipliers, RCA 4832, with extended red photocathodes; amplifiers and electronics to process the photomultiplier signals.

The polychromator has ten channels each 30 A wide, a spread suitable for measuring temperatures in the range from 5 to 300 eV. There are three sets of ports for the laser scattering set at different major radii. Photodiodes monitor beam power and timing.

The He-Ne interferometer (Appendix C) is a Michelson configuration and uses feedback stabilization to eliminate the effects of acoustical and mechanical vibrations. The stabilization is routinely good to 1/100 of a fringe (it can be tuned with care to hold to 1/1000 fringe). For 6328 one fringe corresponds to a line density of $1.8 \times 10^{17}/cm^2$, ($N_e \ell = 4.9 \times 10^{14} \Delta\phi$, degrees) so line densities as low as $2 \times 10^{15}/cm^2$ can be measured. There are small holes in the cusp windings to allow the beam through at twelve different major

radii, producing a nearly continuous radial scan.

Because the vacuum vessel is glass, it can provide easy optical access to the entire plasma volume. Probes 1/2" in diameter are slid between the glass and the windings. A small mirror deflects light from the plasma through a focusing lens and onto the polished end of a fiber light guide bundle. The field of view is narrow, about 5°, and ample light is collected.

Light from the fiber bundle is directed to the slit of a 16 channel polychromator. The polychromator is a modification of a Spex 3/4 meter Czerny Turner monochromator. A cylindrical lens focuses the exit plane onto an array of plastic light guides which carry light to 16 RCA 4840 photomultipliers. Channels are .39 A apart in second order.

A Rogowski belt is fitted between the glass vessel and the windings, oriented to measure the net toroidal current (induced by the preionizer and multipole fields). A diamagnetic loop in the same orientation gives the total toroidal flux in the vessel.

Small magnetic pickups (2.5 x .7 cm), in quartz probes, measure internal fields. They have 15 turns for an nA of 2.6 $cm^2$. Their inductance is low enough to permit measurements at frequencies up to 10 MHz. With the measured parameters, the probes should not seriously interfere with the plasma.

DATA

Thomson Scattering

Figure 9 shows some typical waveforms for the Thomson scattering experiments. Depicted are scope traces, at 200 nsec/cm sweep speed, showing scattered light in the two channels nearest 6943. The background fluctuations are from plasma light. When factor for scope gain and photomultiplier sensitivity are included, the ratio of channel 1 to channel 2 is 5.6:1 and implies a temperature of 5.5 eV. At this temperature, no scattering in channel 3, or in higher channels, would be seen, and, in fact, none was observed. This particular shot was taken at the peak amplitude of the cusp field. One might expect densities and temperatures to be at peak values, or close to them, at this time.

Under no conditions, in Tormac IV, were scattered signals seen in more than the first two channels. For the level of plasma light observed, this would place an upper bound on electron temperature of around 10 eV. No temperatures even this high were seen. If data for the first two channels are fit to a gaussian, the result can be summarized by the expressions.

$$T_e = \frac{9.5}{\ell nR} \qquad R = \text{ratio of intensities of channel 1 to channel 2.}$$

$$\Delta T_e = \frac{9.5 \Delta R}{R(\ell nR)^2}$$

For the example given above $R = 5.6 \pm 2$ implying $T_e = 5.5 \pm 1$ eV. This is quite representative of data taken at the peak of the cusp.

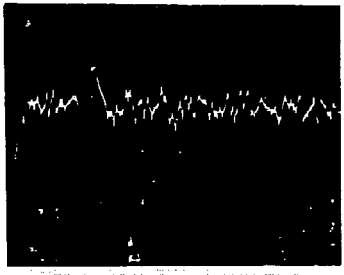

CHANNEL 1
VERTICAL 10 mV/cm
HORIZONTAL 200 nsec/cm
SENSITIVITY 44

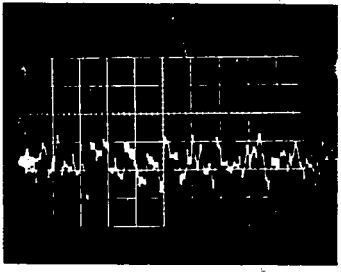

CHANNEL 2
VERTICAL 50 mV/cm
HORIZONTAL 200 nsec/cm
SENSITIVITY 340

Typical Thomson Scattering Data, taken at the peak of the cusp field. The scattering signal is seen a little more than 2 cm from the start of the trace. When corrected for photomultiplier sensitivity, the ratio of channel 1 to 2 is 5.6 implying an electron temperature of 5.5 eV.

XBB 7812-15259A

Fig. 9

Before peak compression, temperatures are lower. The lowest temperature observable with the present apparatus is about 4 ev. These temperatures are reached at 3 μsec before peak compression. No temperatures could be measured at earlier times. Within 3 to 6 μsec after peak compression, electron temperature had fallen to these levels once again. No measurements at later times could be made. Figure 10 summarizes these results.

The gas fill was varied from 17 mTorr to 100 mTorr; data were taken at 17, 34, 51, and 100 mTorr. The intensity of scattering increased steadily, from 17 to 51 mTorr and remained constant when the fill pressure was raised to 100 mTorr. For the lower three pressures, measured temperatures were approximately the same; in the range 4 to 6 eV, possibly highest at 34 mTorr but not significantly so. Temperatures for the 100 mTorr runs were below the 4 eV threshold. Changing the gas mixture from 85:15 $D_2$:He to 100% $D_2$, made no difference in the observed temperature, or in scattering intensity. Raising the cusp voltage from 15 to 17 kV had no noticeable effect either.

At these low temperatures one must consider the effects of cooperative scattering, even at $90^{\circ}$. Using $T_e$ in the range 4 to 6 eV, and estimating $n_e$ (see below) to be 5 to 8 x $10^{15}/cm^3$, we find

$$\alpha \equiv \frac{1}{k\lambda_o} = 10^{-8} \left(N_e/T_e\right)^{1/2} \approx .30 \text{ to } .47$$

The spectrum will be only slightly modified. Actual temperatures

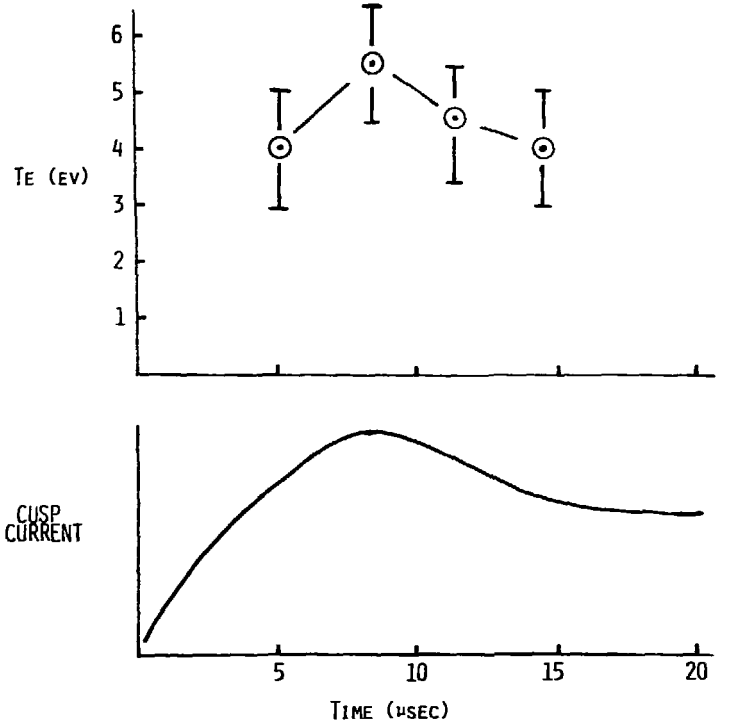


ELECTRON TEMPERATURE vs TIME

XBL 789-10851

Fig. 10

will be less than those calculated as above, for purely incoherent scattering we can calculate the first correction to a gaussian using Salpeter's results[29,30]

$$S(k, \omega) \sim e^{-x^2} [1 - \frac{\alpha^2}{2} W(x) + \ldots]$$

where

$$W(x) = 1 - 2xe^{-x^2} \int_0^x e^{x'^2} dx'$$

$$x = \frac{\omega_o}{\sqrt{2}kv_e}$$

in our experiment channel 1 corresponds to $x_1 = 2.3/\ Te(eV)$ and channel 2 corresponds to $x_2 = 3.9/\ T_e(eV)$. In the extreme case $T_e = 4$ eV and $n_e = 8 \times 10^{15}$ we find

$$\alpha = .47 \qquad \frac{\alpha^2}{2} = .11$$

$$x_1 = 1.16 \qquad x_2 = 1.95$$

$$W(x_1) = 1 - 2(1.16)e^{-(1.16)^2} \int_0^{1.16} e^{x^2} dx$$

$$= 1 - 1.40 = -.40$$

$$W(x_2) = 1 - 2(1.95)e^{-(1.95)^2} \int_0^{1.95} e^{x^2} dx$$

$$= 1 - 1.32 = -.32$$

so

$$1 - \frac{\alpha^2}{2} W(x_1) = 1.04$$

$$1 - \frac{\alpha^2}{2} W(x_2) = 1.03$$

Thus the correction terms are small, their ratio is close to unity and their effect on the temperature calculation is negligible. For more moderate choices of $n_e$ and $T_e$ the effect is even smaller.

These measurements of electron temperature should reflect the local value of ion temperature as well, since at $T_e$ = 5 eV and $n_e$ = 5 x $10^{15}$; electron-ion equilibration times (using Spitzer)

$$\tau_{ie} = 3.2 \times 10^9 \, N_e \, \ell n\lambda / A \, T_e^{3/2}$$

are approximately 60 nsec. This is much shorter than the rise or fall of the cusp field.

He-Ne Interferometer

Figures 11 a-i show results of measurements with the He-Ne interferometer. Plotted, are profiles of $\int n_e \, dl$ vs major radius at several times, $\int n_e \, dl$ vs time for several radii, and total ionization vs time. These plots are shown for cases with and without the cusp field. There was additional data taken at lower fill pressures. Results under those conditions do not vary drastically from the ones shown.

The preionizer ionizes 57% of the gas in the vessel. Ionization is first measurable in the center of the vessel and rapidly builds, peaking at first near the center, then quickly spreading to fill the vessel uniformly. Application of the

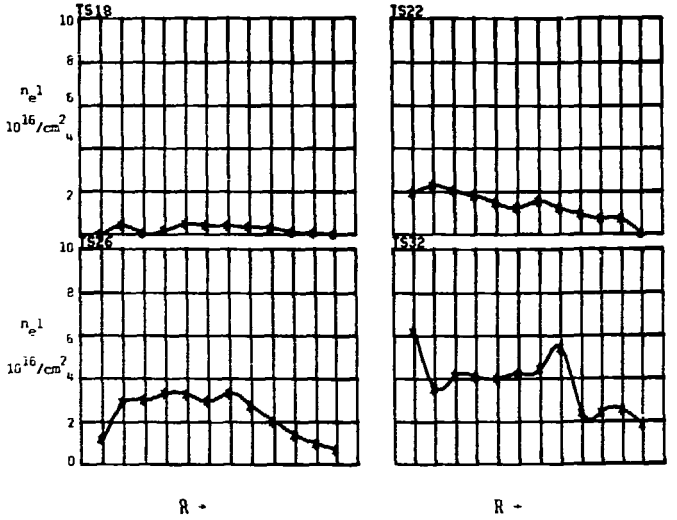


Profiles of $\int n_e \, dl$ vs R at four times. Times are given above each graph. Each horizontal division represents 1 cm. Fill pressure was 36 mTorr.

XBL 789-10865

Fig. 11a

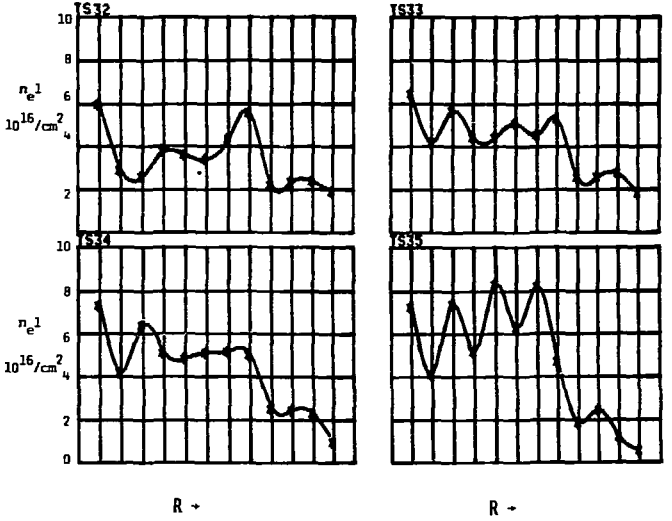


Profiles of $\int n_e \, dl$ vs R at four times. Times are given above each graph. Each horizontal division represents 1 cm. Fill pressure was 36 mTorr.

XBL 789-10867

Fig. 11b

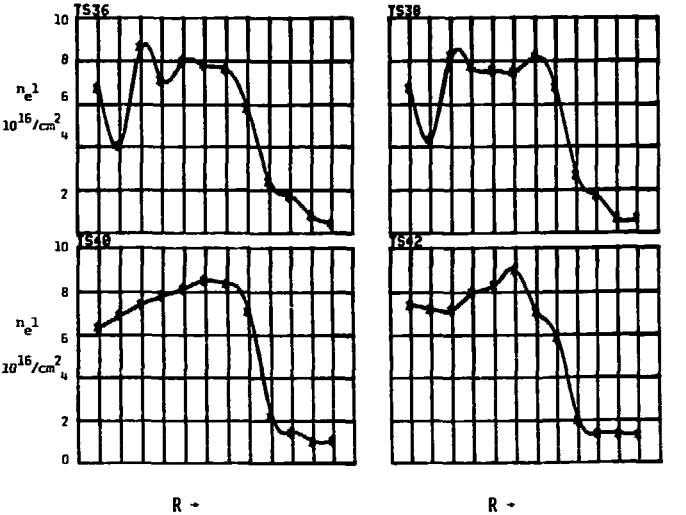


Profiles of $\int n_e \, dl$ vs R at four times. Times are given above each graph. Each horizontal division represents 1 cm. Fill pressure was 36 mTorr.

XBL 789-10868

Fig. 11c

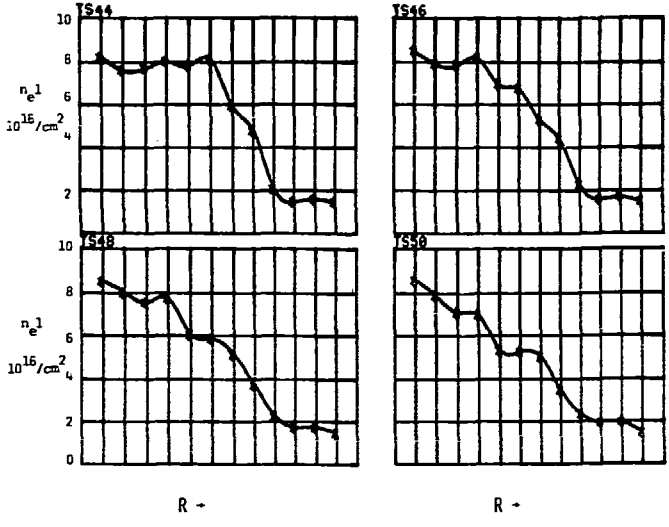


Profiles of $\int n_e \, dl$ vs R at four times. Times are given above each graph. Each horizontal division represents 1 cm. Fill pressure was 30 mTorr.

XBL 789-10869

Fig. 11d

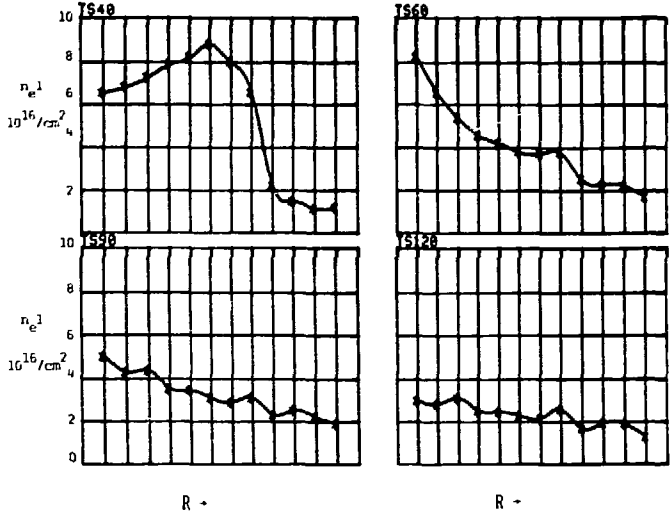


Profiles of $\int n_e \, dl$ vs R at four times. Times are given above each graph. Each horizontal division represents 1 cm. Fill pressure was 36 mTorr.

XBL 789-10870

Fig. 11e

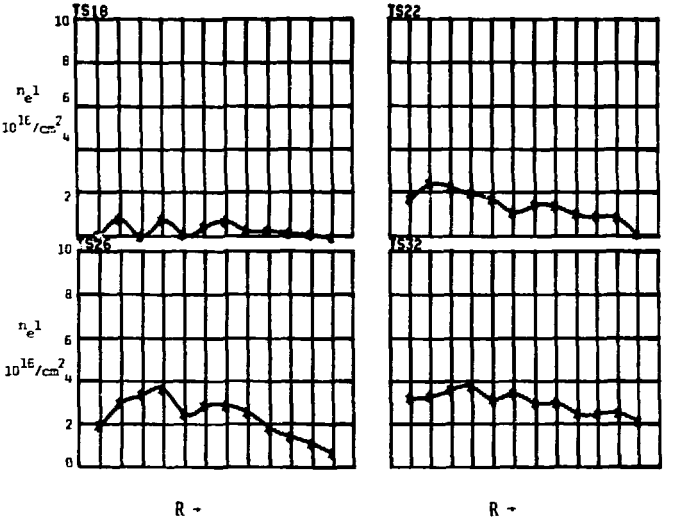


Profiles of $\int n_e \, dl$ vs R at four times. Times are given above each graph. Each horizontal division represents 1 cm. Fill pressure was 36 mTorr. No cusp fields were applied.

XBL 789-10864

Fig. 11f

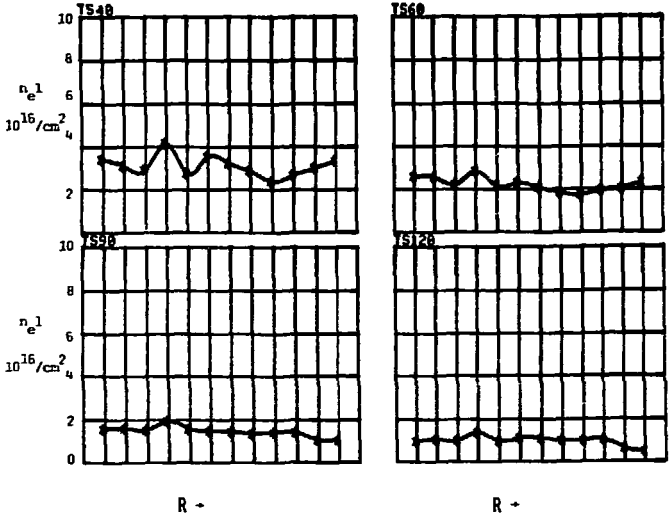


Profiles of $\int n_e \, dl$ vs R at four times. Times are given above each graph. Each horizontal division represents 1 cm. Fill pressure was 36 mTorr. No cusp fields were applied.

XBL 789-10866

Fig. 11g

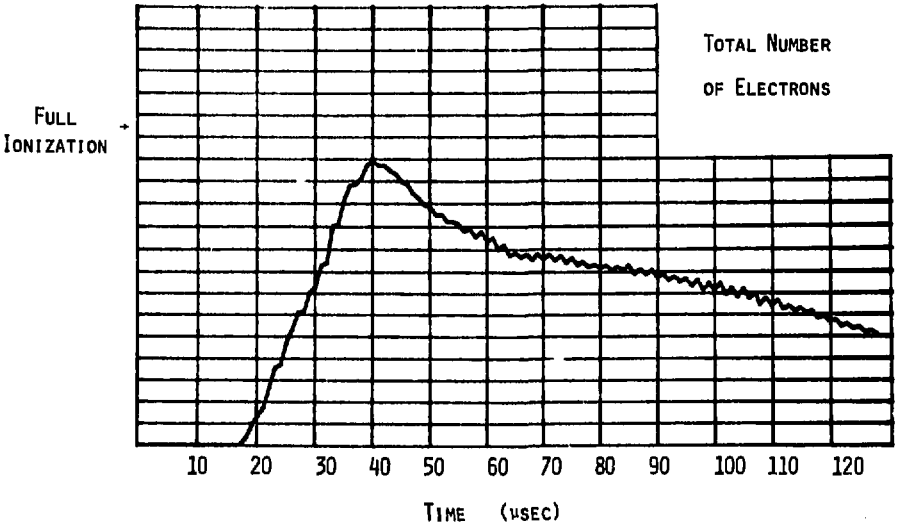


Total ionization vs time. Level of full ionization is indicated. Fill pressure was 36 mTorr.

Fig. 11h

XBL 789-10874

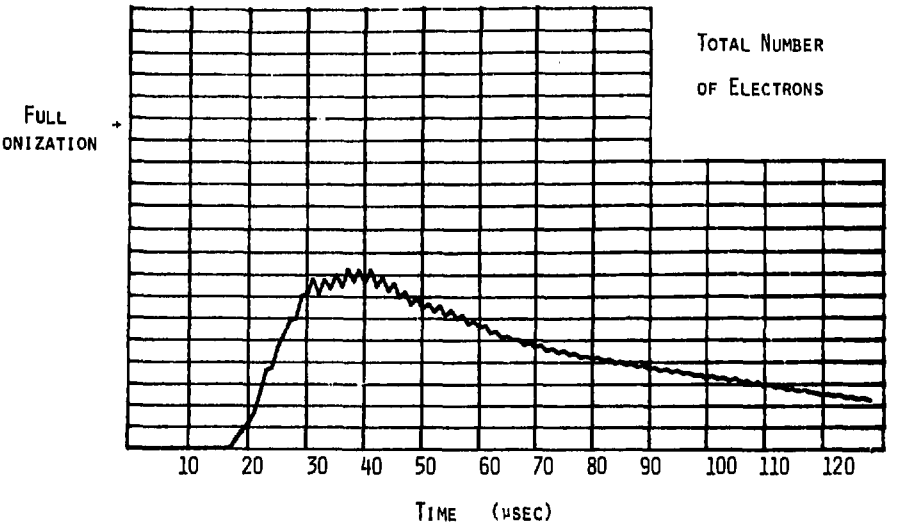


Total ionization vs time. Level of full ionization is indicated. Fill pressure was 36 mTorr. No cusp fields were applied.

XBL 789-10880

Fig. 11i

cusp increases overall ionization to 90%. Density increases dramatically at small major radius and actually decreases at large radii, indication that the poloidal field is pushing the plasma away from the outer wall. There is no indication that the toroidal field has any such effect at the inner wall. At peak compression, the density profile is fairly flat from 7.5 to 17 cm major radius and decreases rapidly at large values. The scale length for this transition region is approximately 1.5 cm at this time. The density is approximately 50% above full ionization, indicating a weak radial compression. Soon after the cusp peak, the gradient decreases and the plasma decays away.

Measurements of density vs "Z" were not possible with the present apparatus and thus one is not able to determine what structure, if any, exists in this direction. If one assumes that there is approximately equal compression in Z and R, 50% in each case, one calculates a volume compression of a little more than two. Average density for this compressed plasma would be $5 \times 10^{15}/cm^3$ and if the profile were peaked, maximum density might fall in the range $7$ to $8 \times 10^{15}/cm^3$. The plasma would be approximately 15 x 10 cm in cross section.

Spectroscopy

HeII 4686

Scans parallel to the center axis at different values of major radius and perpendicular to the center axis at different

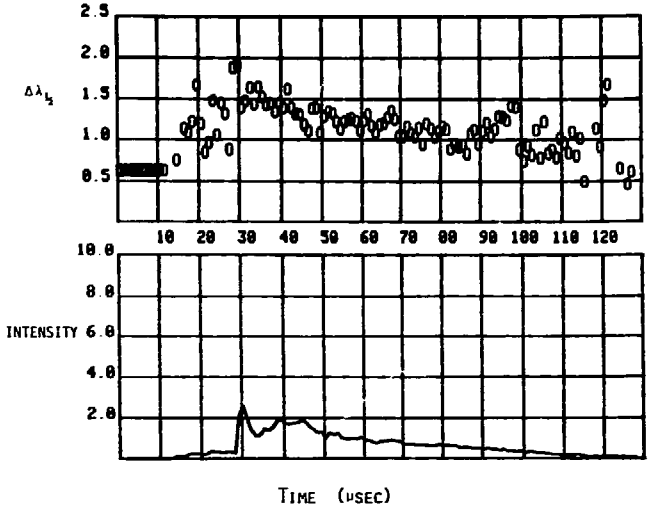


WIDTH AND INTENSITY OF HEII 4686 VS TIME
Z= -5 CM

XBL 789-10855

Fig. 12a

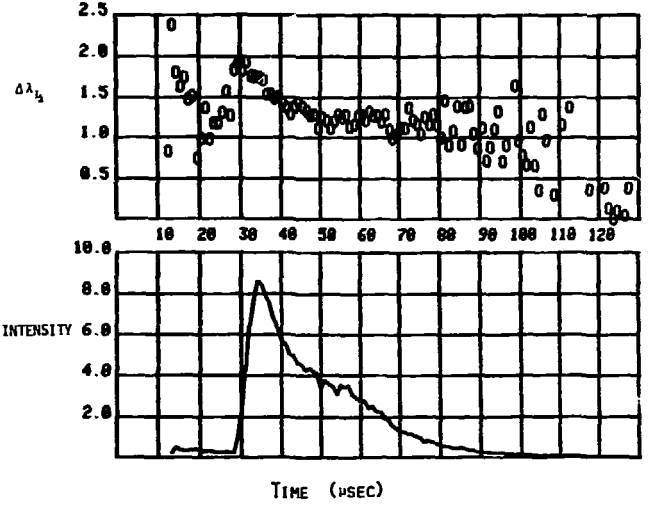


WIDTH AND INTENSITY OF HEII 4684 LINE VS TIME.
Z= 0 CM

XBL 789-10856

Fig. 12b

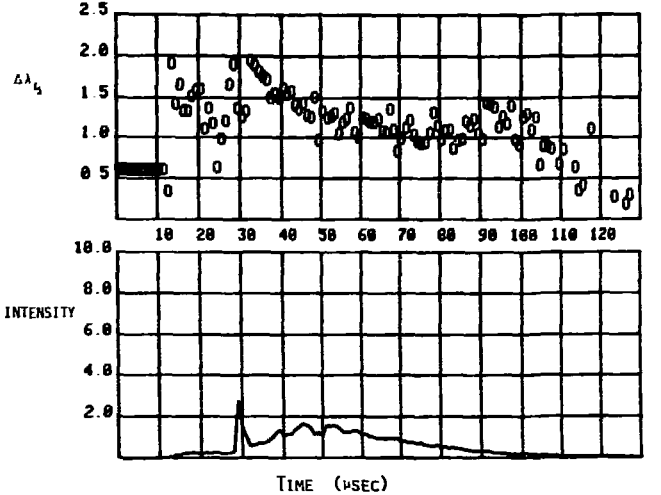


WIDTH AND INTENSITY OF HEII 4686 LINE VS TIME.
Z= +5 CM

XBL 789-10857

Fig. 12c

values of Z were taken of the 4686 line of ionized helium. The 16 channel polychromator and the reticon data collection system recorded time and wavelength resolved data at ten radial positions and twenty Z positions. Figures 12 a-c show typical data; line shape and total intensity are plotted. The lines are fitted to a gaussian

$$I = A\, e^{-\left(\frac{\lambda - B}{C}\right)^2} + D$$

and the best fit to the four parameters are found.

A number of features are obvious. The intensity is peaked at peak compression and falls rapidly thereafter. A small amount of 4686 light is seen during the preionization. It consists of a sharp burst of light, lasting about a microsecond and occuring shortly after the onset of ioniza tion. It can be correlated with a single, half cycle of preionization current. Emission is quenched quickly there-after and little light is seen until the application of the cusp fields. Under some circumstances application of the cusp will lead to a sharp spike of 4686 emission followed by a slower increase and decrease. This feature is most notice-able at high fill pressures and near the vessel center.

Because 4686 is emitted by an ionized species, its inten-sity will follow, to some extent the density of the ion and thus reflects the process of ionization, as well as exci-tation, that occur within the plasma. Some of the atomic physics relating to 4686 emission, and a partial explanation of

the data are included in a later section.

The 4686 widths vary from less than one Angstrom to a little more than two, two Angstroms being a typical value at the cusp peak and one Angstrom typical for later times, 50 μsec after the peak of the cusp. The fall is monotonic. At early times, the light levels are too low to get reliable fits, the same holds true for very late times. There are however, strong indications that 4686 is wide during the brief burst of emission that accompanies preionization. Further study is indicated. At any given time, the width of the line is fairly uniform around the vessel. That is, all lines of sight show similar patterns and time history for the line broadening despite the differences in the patterns of intensities that are seen.

If the line widths are attributed to doppler broadening from ion thermal motion, the temperature corresponding to 2.0 A is 120 eV, at peak compression

$$\frac{\Delta\lambda}{\lambda} = \frac{v}{c} \; ; \quad \Delta\lambda = \sqrt{\frac{T_i}{mc^2}}\,\lambda$$

falling to 25 or 30 eV at later times. The discrepancy between this observation and the Thomson scattering measurement is apparent. At the densities that exist in TORMAC IV, electron-ion equilibration should be rapid.

If one assumes the temperature is low, as indicated by the scattering and instead attributes the line widths to

stark broadening corresponding to electron densities, one finds;

$$\Delta\lambda = 1.79 \times 10^{-11} n^{2/3} \ (\text{Å})$$

$$n = 1.3 \times 10^{16} (\Delta\lambda)^{3/2} \ \text{cm}^{-3}$$

The density will peak at $5.2 \times 10^{16}/\text{cm}^3$ and fall to $1.3 \times 10^{16}$. These values are not compatible with the interferometer measurement and as we will see, with observation of light from neutral hydrogen. The observed width may be the result of the combined effect of doppler and stark broadening corresponding to values of temperature and density lower than those quoted above. Unfortunately, the resulting values are not much more in line with other observations, since the combination of the two effects always implies a higher pressure than one by itself. For example, a 2.0 Angstrom width may be the result of an ion temperature of 50 eV, and a density of $1.5 \times 10^{16}$. Zeeman splitting, fine structure, and instrumental broadening are much too small to account for this excess line width. Combined and properly substracted (by deconvolution) from a line of 2.0 Angstroms width, their effect will be less than 2 or 3 cent. A satisfactory explanation of 4686 broadening has not been found in this case. The matter is discussed further in a later section.

DI 4861 ($D_\beta$)

Scans parallel to the center axis at different values of

major radius were taken of the 4861 line (Balmer β of neutral Deuterium). In all cases, the peak intensity is seen shortly after preionization followed by a rapid decrease upon application of the cusp, then a slow increase for 30 or 40 μsecs, and an even slower decay thereafter. In the case where no cusp field is applied, only the initial rise and slow decay are present. The intensity is greater at small major radius and decreases monotonically at large radius.

One can fit the $D_\beta$ lines to Gaussian or Lorentzian shapes and examine the variation of the width with time and position. One finds, as a general feature, that the widths increase slowly during ionization, remain constant during the cusp rise, then increase over a period of 5 to 10 sec after the cusp peak; doubling in width during the period from 3 or 4 Angstroms to 6 or 7. Afterwards, there is a slow monotonic fall, the widths declining to 3 Angstroms after 60 μsec. There is some variation in this picture at larger major radii, the major differences being narrower lines and less dramatic rise upon application of the cusp. This observation is consistant with the earlier one, that there is simply less plasma at large radii.

Line widths, interpreted as Stark broadening from electron density, are plotted in Figures 13 a-c. Densities calculated in this manner are roughly in agreement with those inferred from the interferometer. Density at the end of preionization varies from $3 \times 10^{15}$ at small radius to

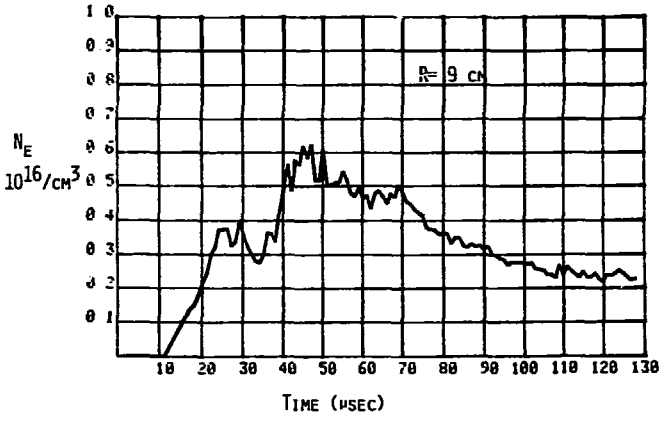


ELECTRON DENSITIES AT R = 9CM INFERRED FROM $D_\beta$ LINE BROADENING VS TIME. THE CUSP RISE BEGINS AT 25 μSEC AND PEAKS AT 33 μSEC.

XBL 789-10854

Fig. 13a

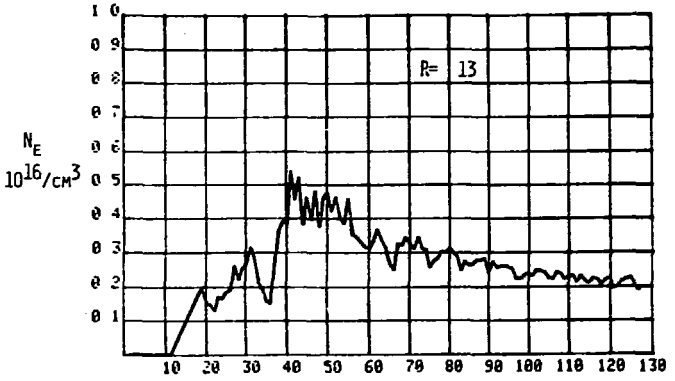


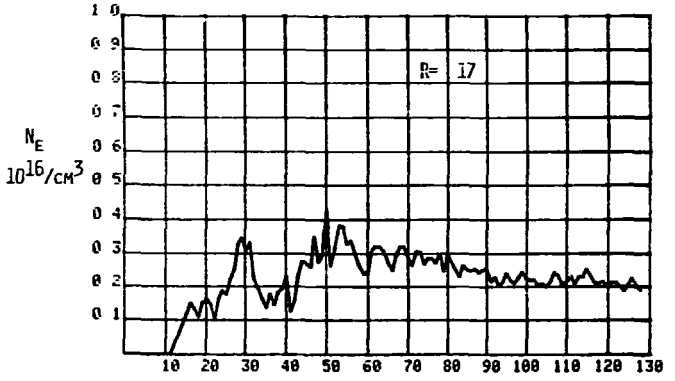


ELECTRON DENSITIES AT R=17 CM INFERRED FROM $D_B$

XBL 789-10853

Fig. 13b

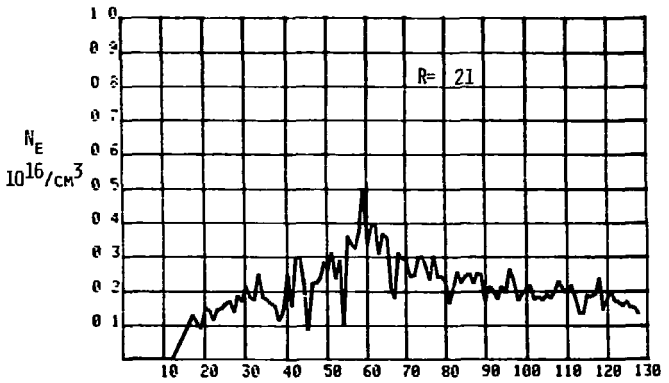


ELECTRON DENSITIES AT R=21 CM INFERRED FROM $D_\beta$

XBL 789-10852

Fig. 13c

$2 \times 10^{15}$ (35 mTorr fill pressure). However, the $D_\beta$ measurement is weighted by the emission intensity, $n^2$ times a function of temperature, so strict quantitative comparison is not simple.

Application of the cusp causes an apparent increase in density, particularly near the inner wall. Peak values are 6 to 7 $\times 10^{15}/cm^3$. Once again we have rough agreement with interferometer data which shows $\int n_e \, dl = 1 \times 10^{17}$ at this value of R. Keeping in mind possible sources of error, non-uniform emission, and alternate sources of line broadening; we can obtain an approximate size for the plasma; 10 to 20 cm.

HeI 5876, 4471

Emission of neutral helium, particularly the 5876 line, was studied. The intensity patterns were similar to those of $D_\beta$ , and the lines were narrow, down at the instrumental limit of .4A. Neutral helium lines have, in general, very small stark coefficients; they are broadened mainly by the Doppler effect. Helium neutrals will not penetrate far into a plasma. The integrated rate coefficient for collisional ionization of helium by a 5 eV plasma is $8 \times 10^{-11}$ $cm^3/sec$ at electron densities of $5 \times 10^{15}$; the ionization time,

$$\tau_I = \frac{1}{n_e \langle \sigma v \rangle_I} = 2.5 \times 10^{-6} \text{ sec}$$

For room temperature neutrals traveling at $6 \times 10^5$ cm/sec

the penetration depth is 1.5 cm. Helium atoms will charge exchange with helium ions, but only at rates too slow to be of interest here. The question of the neutral Helium penetration is still open, however. The plasma attains a 5 eV temperature only for a short period of time near the peak of the cusp. Density is also sharply peaked and ionization is a function of both parameters. At 3 eV and and $3 \times 10^{15}$ density, $\tau_i$ = 17 μsec. Whether or not the neutral helium emission reflects conditions in the body of plasma it presents no difficulties in the picture of TORMAC IV we are developing.

In contrast to helium, hydrogen neutrals have a much greater likelihood of penetrating the plasma. The ionization rate coefficient is larger, $\sigma V = 6 \times 10^{-10}$ cm$^3$/sec at 5 eV, but hydrogen neutrals can be created with substantial energies by dissociation of the molecule. Their velocity is about $10^6$ cm/sec. Further, the charge exchange cross section for hydrogen is larger than that for ionization so slow neutrals can quickly pick up ion velocities and penetrate more easily. Combined with the higher excitation rates that go with the hotter denser conditions near the plasma center, these effects often lead to substantial hydrogen line emission under conditions where the equilibrium population of neutral hydrogen would be low.

Impurity Lines

A brief search for visible lines of common impurities was carried out. Strong lines of OI, OII, OIII, NI, NII, NIII, CI, CII, CIII, CIV, SiI, SiII, SiIII were looked for and none were seen. It is difficult to draw quantitative conclusions from this observation.

Forbidden Lines

In the presence of strong turbulent electric fields, forbidden lines of neutral helium can be observed. A search for these lines yielded none. The conclusion is that either no turbulent fields are present, or no neutral helium is present in regions where the turbulence exists.

Line to Continuum Ratio

The ratio of line to continuum emission can give an estimate of electron temperature in certain plasma regimes. The conditions for LTE, at least for $D_\beta$ should be satisfied by the plasma and the electron temperature is in a suitable range. When an attempt to make the measurement was made, a number of problems arose. First, there was large shot to shot variation in the continuum intensity. Secondly, there seemed to be an excess of continuum radiation. This was seen in the Thomson scattering measurements as well.

Plasma Current

Figure 14 shows traces of the plasma current measured

by a Rogowski belt around the plasma. During preionization the current oscillates in phase with the current in the preionize coils. No plasma current is seen until after the first half cycle of coil current, then it builds quickly to a peak of 40 kA. The plasma current does not oscillate around zero but has an offset. The offset depends on fill pressure, the higher the pressure, the greater the offset. At 50 mTorr fill, the most commonly used value, offset current was about 10 kA. When the preionize bank was crowbarred in phase with the offset, a net current of 12 kA was measured, decaying in 15 μsecs. If the bank is crowbarred out of phase with the offset, essentially no net current remains. Application of the cusp resulted in little or no net plasma current.

Magnetic Probes

Figures 15 a-c show some typical magnetic probe data. Figures 15d and e show profiles of the field components vs R for Z at the center of the vessel and vs Z for R = 11.5 cm. There are a number of features of interest. Outside the plasma, at large major radius; the poloidal field, with plasma is stronger than the vacuum field. Inside the plasma, at small major radius, the field is near zero for early times, increasing to vacuum value after 2 to 6 μsec. This would seem to be further evidence that the poloidal field has compressed the plasma, pushing it away from the outer wall. No such behavior is seen for the toroidal field near the

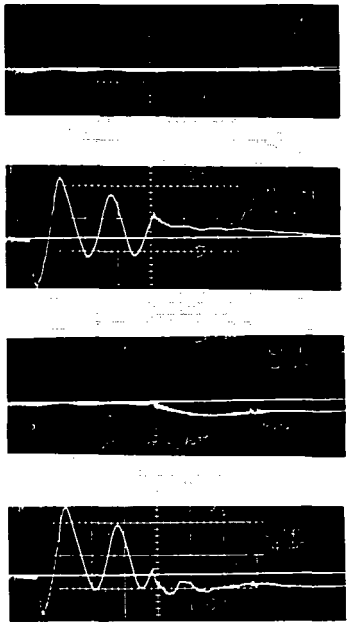


PLASMA CURRENT WAVEFORMS, 23 kAMPS/DIV
CUSP BANK = 15 kV PREIONIZE BANK = 30 kV

XBB 7812-15257A

Fig. 14

inner wall.

The cusp rise is accompanied by strong oscillations in both poloidal and toroidal magnetic fields. These oscillations are strongest at R = 13 cm and extend over a region approximately 3 to 4 cm wide. The toroidal component of the oscillation reaches a peak intensity of 2.5 kG, the poloidal component .9 kG. The period is 2 μsec, approximately an Alfven time across the oscillating region. The oscillation damps rapidly once the cusp reaches its peak.

The oscillations can be correlated with fluctuations in emission intensity of the 4686 line. This may simply be an indication of field and plasma compression. The line width and center are not seen to change. The background intensity, which actually is a measure of the non-gaussian wings of the line (the continuum level being much smaller) also oscillates.

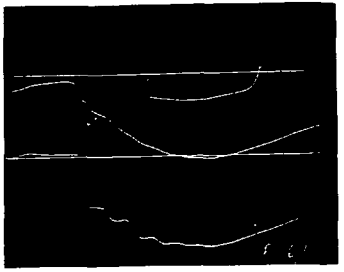

PLASMA SHOT
36 MICRON GAS FILL

$B_T$ 774 GAUSS/DIV

$B_Z$ 866 GAUSS/DIV

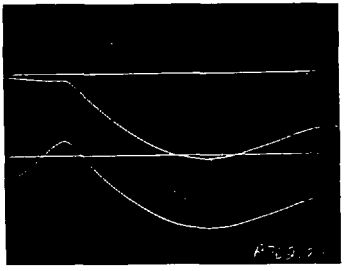

VACUUM SHOT

$B_T$ 774 GAUSS/DIV

$B_Z$ 866 GAUSS/DIV

SMALL PROBE WAVEFORMS, NEAR OUTER WALL
R = 20 CM. Z = 0 CM.
CUSP BANK = 15 KV
HORIZONTAL 2 USEC/DIV

XBB 7812-15263A

Fig. 15a

PLASMA SHOT
36 MICRON GAS FILL

$B_T$ 1935 GAUSS/DIV

$B_Z$ 433 GAUSS/DIV

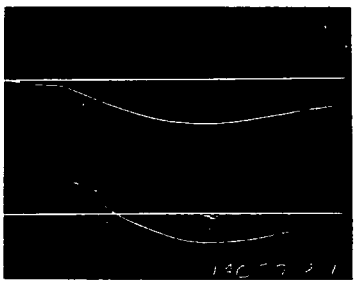

VACUUM SHOT

$B_T$ 1935 GAUSS/DIV

$B_Z$ 433 GAUSS/DIV

SMALL PROBE WAVEFORMS, NEAR CENTER
R = 15 CM. Z = 0 CM.
CUSP BANK = 15 KV
HORIZONTAL 2 USEC/DIV

XBB 7812-15262A

Fig. 15b

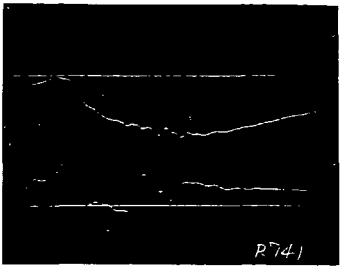


PLASMA SHOT
36 MICRON GAS FILL

$B_T$ 1935 GAUSS/DIV

$B_Z$ 433 GAUSS/DIV

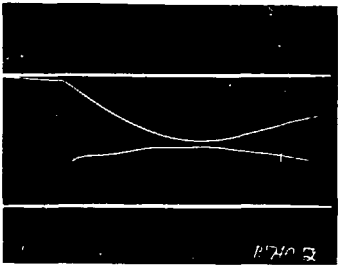


VACUUM SHOT

$B_T$ 1935 GAUSS/DIV

$B_Z$ 433 GAUSS/DIV

SMALL PROBE WAVEFORMS, NEAR INNER WALL
R = 10 CM. Z = 0 CM.
CUSP BANK = 15 kV
HORIZONTAL 2 USEC/DIV

XBB 7812-15261A

Fig. 15c

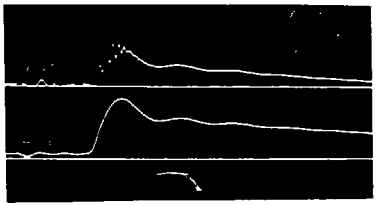

SMALL PROBE MEASUREMENT OF TOROIDAL FIELD IN PLASMA, AT R=13.9 CM
2000 GAUSS/DIV

FLUX LOOP
VERTICAL 1V/DIV
HORIZONTAL 10 USEC/DIV

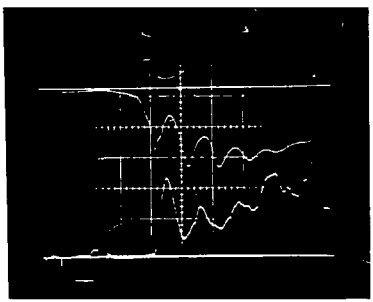

SMALL PROBE, $B_T$
774 GAUSS/DIV

4686 Å INTENSITY
HORIZONTAL 2 USEC/DIV

FLUCTUATIONS IN TOROIDAL FIELD AND 4686 Å EMISSION DURING CUSP CURRENT RISE.

XBB 7812-15258A

Fig. 15d

*DISCUSSION*

Plasma Temperature

We would like to understand the measured temperatures in terms of the processes that are occuring in the plasma. First, we note that the plasma is highly collisional. Below, various collision frequencies and transport coefficients for both the preionized plasma and for the compressed plasma are tabulated.

We can make a reasonable estimate of the preionized plasma temperature by noting that it is high enough to maintain significant ionization of the hydrogen component (demonstrated by the $H_\beta$ intensity and measured density) but not high enough to significantly ionize and excite helium (seen by the HeII 4686 intensity). Since the plasma reaches 4 eV only toward the end of compression and since ionization is a strong function of temperature, we can take the preionize temperature to be 2 eV. The density during preionization is about $2 \times 10^{15}$. With these numbers and expressions from the NRL tables[31] we calculate (for $T_i \sim T_e$ in eV). The electron-ion energy equilibration time

$$\nu^{\epsilon}_{ei} = 1.6 \times 10^{-8}\ n_e/T_e^{3/2}$$

$$\nu^{\epsilon}_{ei} = 1.1 \times 10^{7}\ \text{sec}^{-1}$$

$$\tau^{\epsilon}_{ei} = 8.6 \times 10^{-8}\ \text{sec}$$

the ion-ion collision frequency

$$\nu_{ii} = 5.0 \times 10^{-7} \; n_e/T_e^{3/2}$$

$$\nu_{ii} = 3.5 \times 10^{8} \text{ sec}^{-1}$$

$$\tau_{ii} = 2.8 \times 10^{-9} \text{ sec}$$

the electron - electron collision frequency

$$\nu_{ee} = 3.0 \times 10^{15} \; n_e/Te^{3/2}$$

$$\nu_{ee} = 2.0 \times 10^{10} \text{ sec}$$

$$\tau_{ee} = 4.7 \times 10^{-11} \text{sec}$$

for comparison

$$\Omega_i = 6.8 \times 10^{6} \; B(kG)$$

$$\Omega_e = 1.8 \times 10^{10} \; B(kG)$$

classical resistivity

$$\eta = 1.15 \times 10^{-14} \; n_e/Te^{3/2}$$

$$\eta = 4.1 \times 10^{-14} \text{ sec}$$

For the compressed plasma $n_e = 5 \times 10^{15}/cm^3$ $T_e = 5$ eV

$$\nu_{ei}^{c} = 7.1 \times 10^{6} \text{ sec}^{-1}$$

$$\tau_{ei}^{c} = 1.4 \times 10^{-7} \text{ sec}$$

$$\nu_{ii} = 2.2 \times 10^{8} \text{ sec}^{-1}$$

$$\tau_{ii} = 4.5 \times 10^{-9} \text{ sec}$$

$$\nu_{ee} = 1.3 \times 10^{10} \text{ sec}^{-1}$$

$$\tau_{ee} = 7.4 \times 10^{-11} \text{ sec}$$

$$\eta = 1.0 \times 10^{-14} \text{ sec}$$

The low temperature during preionization is not surpirsing. The ionize bank contains 900 joules. By comparing

the damping rate of the ionize current, with and without plasma; we find that a third or 300 joules is dissipated in the plasma. The vessel has a volume of $3.2 \times 10^4$ $cm^3$. At a fill pressure of 50 mTorr, corresponding to $3.5 \times 10^{15}$ atoms/cm, we have $10^{20}$ atoms. There is then $300/(1.6 \times 10^{-19})(10^{20}) = 20$ eV/atom. Ionization requires a minimum of 13.6 eV/atom for hydrogen 2.2 eV (per atom) for dissociation of the molecule and there are always parasitic losses, excitation, and emission, and losses to the walls. The effect is to hold the temperatures to a value where the ionization rate is sufficient to absorb the ionize bank energy. The ionization rate is given by Wilson and White[33] for hydrogenic species and temperatures in the range $.02 \leq kT/x \leq 100$ where $x$ is the ionization energy, 13.6 eV for hydrogen. From an analytic fit to the cross section $\sigma(v)$ they give for $S \equiv \langle \sigma v \rangle$.

$$S = \frac{1.1 \times 10^{15}}{\chi^2} \frac{T_e}{(6+T_e/\chi)} e^{-\chi/T_e}$$

for hydrogen and $T_e < \chi$

$$S = 10^{-8} T_e e^{-13.6/T_e} \quad cm^3/sec$$

The ionization time $\tau_i = \frac{1}{n_e S}$ and the power absorbed by ionization is $P_I = 13.6\ n_e S$ eV/sec per atom. The preionize bank puts out 20 eV/atom in $5 \times 10^{-6}$ sec. Equating these

$$13.6\ N_e \cdot 10^{-8} T_e e^{-13.6/T_e} = 20/(5 \times 10^{-6})$$

so $T_e e^{-13.6/T_e} = .01$

which is satisfied for $T_e = 2.5$ eV. Electrons and ions will quickly equilibrate.

Because of the high degree of collisionality; we don't expect a localized current sheath during the process. Density and temperature gradients should be fairly mild throughout the plasma.

When the cusp is applied, the electron temperature rises and ionization increases. Absorption of energy by neutrals, through ionization and line emission will not represent the major cooling mechanism but it will be significant. The major cooling mechanism in TORMAC IV would seem to be by electron thermal conductivity along the open field lines. The open poloidal lines quickly penetrate the plasma under the conditions that exist during the cusp rise. Field diffusion is given by

$$\frac{\partial B}{\partial t} = \frac{\eta c^2}{4\pi} \nabla^2 B$$

so

$$\tau_B = \frac{4\pi L_B^2}{\eta c^2} \qquad L_B = \text{scale length for field gradient}$$

$$\eta = \frac{1.1 \times 10^{-14} \ln\Lambda}{T_e^{3/2}} \qquad \text{(classical)}$$

$$\tau_B = 1.3 \times 10^{-7} L_B^2 T_e^{3/2}$$

for $L_B$ = 5 cm, Te = 2 eV

$\tau_B$ = 9 μsecs about equal to the cusp risetime. The evidence from the magnetic probes is that the fields penetrate much more quickly, in less than 4 μsec.

We can calculate parallel heat flow as follows: the heat flux

$$\Gamma_Q = \kappa \nabla T \qquad \kappa = \text{electron thermal conductivity}$$

$$\frac{\partial T}{\partial t} = \nabla \cdot \frac{K}{C_v} \nabla T \qquad C_v = \text{heat capacity}$$

For weak gradients we don't go too far wrong in writing

$$\frac{\partial T}{\partial t} = \frac{K}{C_v} \nabla^2 T$$

$$t_Q = \frac{C_v L_Q^2}{\kappa} \qquad L_Q = \text{scale length for temperature gradient}$$

$$C_v = \frac{n\kappa}{2} \qquad \kappa = \text{Boltzmann constant}$$

from Spitzer

$$\kappa_{\parallel} = \delta_T \, \varepsilon \, 20 \left(\frac{2}{\pi}\right)^{3/2} \frac{kT^{5/2}k}{m_e^{1/2} e^4 z \ell n \Lambda}$$

$$\kappa_{\parallel} = \frac{(.22)(.42)(4.6 \times 10^{-12})}{\ell n \Lambda} \, T(^\circ K)^{5/2}$$

Converting units and combining these equations

$$\tau_Q = \frac{7\times10^{-21}\ nL_Q^2}{T_e^{5/2}(eV)}$$

as an example for $n = 5 \times 10^{15}$, $L = 5$ cm, $T_e \approx 5$ eV

$$\tau_Q = 1.5 \times 10^{-6} \text{ sec} << \text{cusp risetime}$$

We can do the calculation in another manner. The plasma can convert magnetic field energy to particle energy by ohmic heating, dissipating the diamagnetic current. Power per cubic cm available to the plasma is

$$\eta J^2 = \frac{B^2}{8\pi}\frac{1}{\tau_B} \qquad \tau_B \text{ as calculated earlier}$$

We can equate this to the cooling rate calculated above

$$\frac{B^2}{8\pi}\frac{1}{\tau_B} = \frac{3\eta kT_{(erg)}\ T_e^{5/2}}{\eta L_Q^2\ 7\times10^{-21}}$$

$$\frac{B^2}{8\pi}\frac{\eta c^2}{4\pi L_B^2} = \frac{(3)(1.6\times10^{-12})T_e^{7/2}(eV)}{7\times10^{-21}L_Q^2}$$

substituting for $\eta$ and simplifying, we find

$$460B^2(kG)\ \left(\frac{L_Q}{L_B}\right)^2 = T_e^5$$

In our case near the cusp $L_Q \sim L_B$, $B \sim 4$ kG so

so $T_e = (7400)^{1/5} = 6$ eV.

This is a very crude calculation, of course, but the basic result seems sound. If field lines are open to a wall, the very strong temperature dependence of electron cooling will keep the electron temperature low. In our

case, the high density and the absence of the mechanism to heat ions, causes the ions to be cold as well.

Simulation work by M. Vella gave similar results. The code treats the electrons as a fluid and uses particle equations for the ions. It was written by Hamasaki, now at SAI in San Diego, to study fast pinches. For TORMAC IV-like parameters; 4.25 kG rising in 8.3 μsecs, a 300 G bias field, with a starting density of $3 \times 10^{15}$ fully ionized at 1 eV, ion and electron temperatures at the time of peak field were 5 to 10 eV. Peak densities were 6 or $7 \times 10^{15} cm^3$.

Line Intensities

The intensity of line emission should reflect plasma conditions. Although the processes involved, excitation and ionization in an inhomogeneous, rapidly changing plasma are complicated, some conclusions can be reached.

$D_\beta$ emission can be explained simply. During ionization large numbers of energetic electrons are created. These electrons excite neutral deuterium which promptly radiates. Because preionization is far from total, (60%, maximum) there is no shortage of hydrogen atoms. Application of the cusp ionizes most of the remaining gas, decreasing the intensity. As the plasma decays, the light first increases as the number of neutrals increases then decreases as the number and energy of free electrons decreases.

The 4686 emission of helium is not as easily explained. Since its source is an ion, the helium atoms must first be

ionized. At the electron temperatures present in the preionized plasma, no significant helium ionization can take place. At $T_e = 2$ eV, $n_e = 2 \times 10^{15}$ cm$^{-3}$ ionization times approach a thousand μsec. The burst of light seen at this time is probably the product of runaway electrons created early in the ionization process.[37,38] Electrons above a critical energy $\epsilon_c$ will run away in the presence of an electric field given by the expression

$$\epsilon_c \text{ (eV)} = 5.2 \times 10^{-12} \quad n_e/E$$

The field induced by the preionize winding is given by Faradays law

$$\int E \cdot ds = \frac{1}{c} \frac{\partial}{\partial t} \int B \cdot da$$

or $\quad E \cdot 2\pi R = \frac{L \partial I}{\partial t}$ $\quad$ R = major radius

L = inductance of winding

and $\quad E = \frac{L}{2\pi R} \frac{\partial I}{\partial t} = 500 \text{V/cm}$

The density when this burst of lights is seen is $10^{15}$ cm$^{-3}$ so $\epsilon_c = (5.2 \times 10^{-12})\ (10^{15})/500 = 10$ eV .

There should be a substantial number of electrons with these energies. When accelerated above 30 eV rapid ionization and excitation can take place. As density increases and the field decreases the runaway population disappears. Application of the cusp can produce the same effect. In this case

the density is higher, 2 x $10^{15}$, but so is the induced field at 1000 V/cm. As before $\varepsilon_c \approx 10$eV. As the temperature and density rise, thermal ionization begins to become significant. At 5 eV, 5 x $10^{15}$ ionization time for neutral helium is 4 sec.[34]

We do not expect burnout of the singly ionized helium. Ionization times for the process $He^+ \rightarrow He^{++}$ under the conditions in the compressed plasma are about 100 μsec.[32,33]

HeII 4686 Width

As discussed before, neither density or temperature seem to explain the observed width of the 4686 line. A possible source of the excess braodening is coherent fluid motion at Alfven velocities. Ions tied to field lines would be affected. Neutrals would not. At the densities present, field perturbations would need to be almost 3 kG to produce the observed widths. In the probe data oscillations this large were seen at some times and some places. This motion would not imply much energy since at the velocities involved, 4 x $10^6$ cm/sec, $D^+$ ions would have energies of only 30 eV. This motion is two dimensional and must share its energy with three ion and three electron degrees of freedom. Thus only 10 eV per particle is available. Dissipated over 10 to 20 μsec. this would not lead to any significant rise in the plasma temperature.

Some measurements of the 3203 line of HeII were made.

Since it has a lower wavelength, its Doppler width should be smaller. The line is in fact wider by about 50%. However, 3202 has a larger Stark coefficient and electron density will make a large contribution to its width. Clearly more work must be done to clear up this matter.

ACKNOWLEDGMENTS

There is no shortage of people to thank for help and assistance in this work. I would like to thank John Coonrod who shared the work of constructing and diagnosing TORMAC IV-c; Wulf Kunkel, my advisor, for help and advice; Ian Brown, Rory Niland, Ben Feinberg, Mike Vella, Bob Shaw, Booth Myers, Phil Pincosy, Bruno Vaucher, and Mort Levine, my supervisor, who taught me a great deal about experimental physics. I would also like to thank W.I.B. Smith who started me on my way in Thomson scattering. Bob Peterson, Gary Tabler, Gus Saucedo, Eloy Salinas, Joe Holdener, Phil Smith and Jim Galvin of our shop, were invaluable in the work and suggestions they provided on the experiment. Also, I would like to thank Lou Biagi and the personnel of his mechanical shop, Dane Anderberg and his glass shop, Jack Borde of the optical shop and Tina Aitkens, our secretary. Special thanks goes to Dr. M.K. Hudson for much valuable assistance.

## APPENDIX A EXPERIMENTAL DETAILS

### Cusp Windings

The magnetic fields in TORMAC IV-c were made to match those of IV-a as closely as possible. The windings combine poloidal and toroidal components in a single turn solenoid of varying pitch. Inductance is thus kept low and problems of phasing and coupling independent circuits are eliminated.

TORMAC IV-a was designed with the aid of an electrolytic tank, an analog device.[39] Once designed the fields can be plotted in detail by computer. Figure 5a shows lines of constant $\psi = RA_\theta$, poloidal field lines. Figure 5b shows contours of $|B|$, with both toroidal and poloidal components included. The main feature of the Tormac configuration can be seen, a vacuum minimum B and a pair of cusps.

The windings themselves are constructed of one hundred #14 wires in parallel. This should be a sufficient number to keep ripples in the vacuum field negligible. The wires are never more than 1.5 cm apart and should be more than 8 cm away from the plasma at these points. Each wire is 300 cm long; the total resistance of this portion of the circuit is 2.7 mΩ; the total mass of the wire is 6.2 kg. The maximum design current is 500 kA for a 100 microsecond interval. This would deposit 7.0 kJ in the windings and lead to a temperature rise of 3°C. Typical machine operations is at 250 kA. In either case the large exposed surface of the coil should

dissipate the heat in the 2 to 5 minutes between shots.

For ease of construction and assembly, the windings were constructed in four parts. Details can be seen in figure 7. A wooden cylinder served as a form for winding the center section. The cylinder was slightly larger than the glass vacuum vessel and came apart to ease the removal of the finished coil. Before winding began the cylinder was covered with polyethylene sheet and 400 teflon pegs were inserted to aid in forming each wire. Additional teflon plugs were used to preserve spaces through which glass ports would later fit. For mechanical reinforcement the wires were interwoven with fiberglass tape which was laid around and across the coil. When all 100 wires were in place, additional fiberglass was wound around them and the entire coil potted in epoxy resin (Epon 815 with Versamid 140 catalyst) heated to speed curing and rotated during curing to keep the epoxy from dripping or welling.

The two endplates were wound on 1/4" sheets of nema 7G, an epoxy fiberglass composite. The nema was cut into circular annuli with holes to match the laser and pumping ports. Additional holes were drilled as access for the He-Ne interferometer. The nema was sandblasted to roughen one side and preformed wires were laid onto this side. A thick layer of epoxy was poured on, covering the wires. The epoxy bonds very tightly to the roughened nema surface.

A copper pipe through the vessel center completes the

circuit. The three outer sections were formed with each wire attached tightly with lugs and screws. Split copper pipe with larger diameter than the inner cylinder, was soldered to the inside of the annuli. The inner cylinder was slipped through and tightly held with hose clamps. These provide additional support for the soldered wires, as well. Current is fed on one side, a lucite tube insultates the two sides of the circuit.

Figure 9 shows the complete cusp circuit. The bank consists of eight 14 μF capacitors in parallel. They can operate at voltages up to 20 kV for a total energy of 22 kJ. Typically the bank was run at 15 kV or 12.8 kJ of stored energy. Eight #7703 ignitions are used for series switching, one on each capacitor. A bank of four #5555 ignitions serve for crowbarring. The cusp coil is fed with an 8" wide stainless steel stripline. Stainless is used to decrease the L/R time of the crowbarred circuit and reduce mechanical stress on the winding. If plasma conditions warranted it, copper could be substituted to provide longer decay times.

Rise time for the cusp circuit is 8.3 microseconds (T/4) implying an overall system inductance of 250 nH. The calculated inductance for the coil is 160 nH leaving 90 nH as stray series inductance. Fall time after crowbarring is 80 microseconds, implying a crowbarred resistance of 3.5 mΩ , most in the stainless steel stripline.

Preionize Bank and Winding

Ionization is accomplished by ringing a 2 μF capacitor into a pair of single turn toroidal coils placed outside the cusp winding. The capacitor is charged to 30 kV for a bank energy of 900J. The circuit rings at 110 kHz implying a circuit inductance of 1 μF. A #7703 ignitron provides series switching a pair of ignitrons allow for crowbarring at any phase of the oscillation. There is an additional small capacitor used to deliver a high frequency oscillation to a separate pair of coils and aid in initial gas breakdown. It is powered off the large preionize capacitor. The preionize coils are fed by stripline, both coils and stripline are well insulated with layers of mylar and polyethylene. The preionize circuit is shown in Figure 8.

Bias Winding

The bias field is produced by a loosely wound, 8 turn solenoid of heavy insulated cable. It is powered by a 375 μF bank charged to 2 kV producing a 300 G field in the vessel center. It is highly damped and rises in about 200 microseconds.

Mechanical Reinforcements - Windings

Forces generated by the large currents in the Tormac cusp winding must be supported. In the absence of a complete and tedious analysis of the stresses to be supported; we can identify the major forces produced and the amount of reinforcement needed. In all cases we use the maximum design current

of 500,000 amps for the calculations. This will produce forces some four times greater than the normal operating current of 250,000 amps. The fields are applied for a period of approximately 100 microseconds, placing us in an intermediate regime where neither D.C. nor impulse calculations are entirely applicable. Impulse calculations give smaller stresses, so for safe practice, D.C. values are used.

The largest force on the windings is hoop stress coming from the three poloidal field coils. The force is outward, evenly distributed around the circumference.

The force is calculated by taking

$$F = \frac{-\partial u}{\partial r}$$

u = magnetic energy = $1/2\ LI^2$

r = coil radius

at constant loop voltage,

$$-\frac{\partial u}{\partial r} = \frac{-I^2}{2}\frac{\partial L}{\partial r} + \frac{LI}{2}\,2\,\frac{\partial I}{\partial r} = \frac{I^2}{2}\frac{\partial L}{\partial r}$$

for a single loop $L \sim r$ so

$$F = \frac{LI^2}{2r}$$

Summing the three coils

$$F = \frac{2\times10^{-6}}{2}\,\frac{[(.21)^2+(.35)^2+(.21)^2][500,000]^2}{.25}$$

$$= 2.1 \times 10^5 \text{ Nts}$$

$$= 47,000 \text{ lbs}$$

Supporting this force are 100 #14 copper wires and 15 layers of .007" fiberglass tape all impregnated with epoxy.

Using values of tensile strength from the CRC tables[40] we find

.48 sq inches copper @ 30,000 PSI = 15,000 lbs

1.05 sq inches fiberglass @ 6,000 PSI = 65,000 lbs

There is a safety factor of almost two.

Adjacent hoops have strong forces pushing them apart (their currents are in opposing direction). The force per unit length between 2 current carrying wires is

$$F/\ell = 2 \times 10^{-7} \frac{I_1 I_2}{r} = \frac{(2\times10^{-7})(.21)(.35)(500,000)^2}{.09}$$

$$= 4.1 \times 10^4 \text{ Nts/M}$$

Summed along the circumference 2 R = 1.56 M

$$F = 6.4 \times 10^4 \text{ Nts} = 14,000 \text{ lbs.}$$

This force is somewhat mitigated by the third coil. Forces on the center coil are more or less balanced. Outward force on the outer coil is reduced by about 25%. To support this force six layers of epoxy impregnated fiberglass tape were laid across the coil and interwoven between toroidal wires. Its strength

(.007" x 6)(2π x 10")(60,000 PSI) = 160,000 lbs

much greater than 14,000.

Forces on the endplates are primarily outward. For the case of a circular annulus, 1/4 " thick and 9" in diameter, with uniform loading of 4 ATM (this corresponds to .5MA in

the coils) and supported along its inner and outer radius, the maximum stress is given by formulas in Roark as 6,400 PSI (see fig 16 for more details). The nema will easily support up to 30,000 PSI.

There is a tendency for individual wires of the coil to pinch together. The forces involved are approximately

$$F/\ell = \frac{(2\times10^{-7})(.38)(5000)(500{,}000)}{2}$$

$$= 10{,}000 \text{ nts/M} = 54 \text{ lbs/inch}$$

and are easily supported by weaving fiberglass between wires and impregnating them with epoxy. Forces on the preionizer and bias windings are very small and are easily supported by the conductors and their insulation.

Vacuum System

A schematic of the vacuum system is given in Figure 17. The vessel has a pumping port 1.5" in diameter, 6" in length. These dimensions set the limit on conductance for the overall system. Using standard formulas for air in molecular flow (valid for $p < 10^{-4}$ torr) conductance through long vacuum pipes,[42]

$$U = 116\pi r^3 \frac{8}{3L}$$

U = conductance ($M^3$/sec)
r = pipe radius (M)
L = pipe length (M)

For the pumping port $U = 3.0 \times 10^{-2} M^3$/sec.

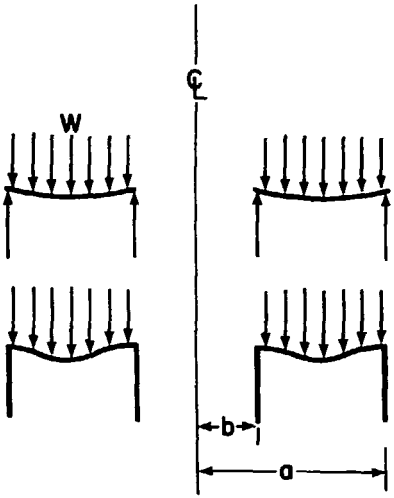


# Geometry for stress calculations uniform loading on annular ring

XBL 789-2204

THE MAXIMUM STRESS ON A UNIFORMLY LOADED ANNULUS IS RADIAL AND IS GIVEN BY THE EXPRESSION $S_R = 6KwA^2/T^2$ . W IS THE LOADING IS LBS, A IS THE OUTER RADIUS IN INCHES, AND T IS THE THICKNESS OF THE ANNULUS. FOR B/A = .3 K = .055 .

Fig. 16

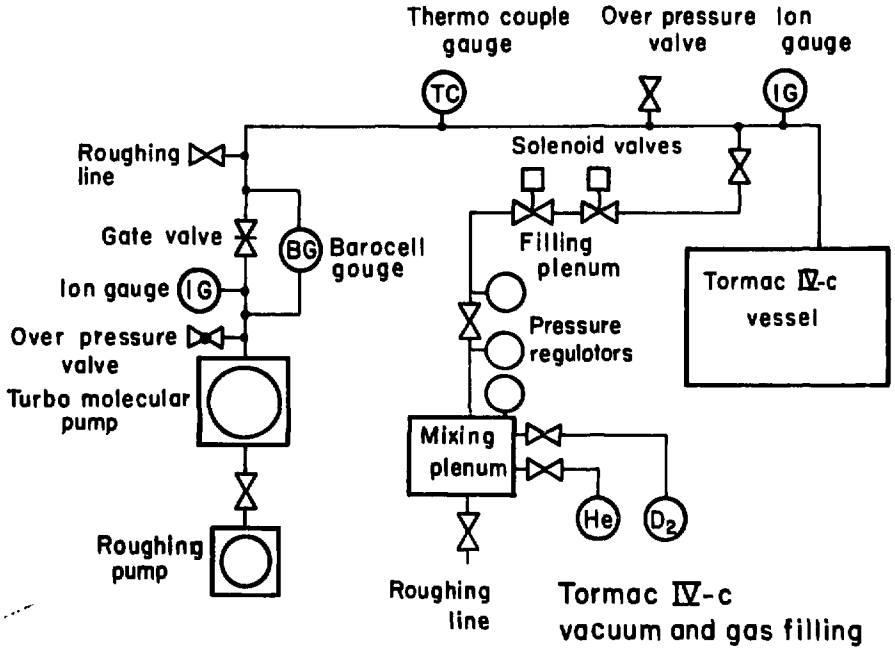


Fig. 17

XBL 789-2209

The vessel is connected to the pump by a large stainless steel manifold. Conductances of pipes in series add like electrical conductances, that is like resistors in parallel. If the manifold is made with sufficiently large diameter it will not further impede the pumping. The manifold is 48" long, 4" in diameter for a conductance of $9.7 \times 10^{-2}$ $M^3$/sec. The next smallest standard size of tubing is 3" giving a conductance of $4 \times 10^{-2}$ which is too small. A 6" tube gives $3.2 \times 10^{-1}$. The 4" pipe was chosen as a good compromise between conductance and convenience; the advantage in using 6" pipe was not sufficient to offset its bulk and weight. The overall system conductance is $2.3 \times 10^{-2}$ $M^3$/sec. The pumping speed at the throat of the turbomolecular pump is .26 $M^3$/sec giving a ratio of vessel pressure to pump pressure of .26/.023 = 11. Typically, pressure at the pump was $5 \times 10^{-8}$ torr, implying a vessel pressure of $5.5 \times 10^{-7}$ torr. The calculations could be checked against an ion gauge which measured pressure at the end of the manifold and were in reasonably good agreement.

The vessel was filled with a mixture of $D_2$ and He. Fill pressures for the experiment ranged from 10 to 100 mTorr, about five orders of magnitude above base pressure in the vessel. The filling system consists of a large mixing plenum with a gauge to measure the partial pressures of the two gases, a one stage regulator to set the pressure on the fill plenum, and the fill plenum itself, isolated by a pair of solenoid valves. Before the mixing plenum is charged, the entire

system is roughed all the way back to the high pressure valves on the gas bottles. The mixing plenum is valved off from the pump and the filling regulator and filled with $D_2$ and He. The lines to the gas bottles are valved off, leaving positive pressure in their lines to avoid contamination if a small leak exists. The regulator to the filling plenum is opened and set to the desired pressure, typically 7 PSI. Operation of the solenoids in sequence will discharge a small quantity of gas into the vessel. Fill pressure is measured with a barocell, an electric manometer. The two arms of the barocell are attached on either side of the gate valve. To vary the filling pressure the filling plenum can be charged and discharged several times or the pressure in the plenum can be adjusted.

The vacuum system provides for roughing and backfilling separately on both sides of the gate valve. Argon is generally used for backfilling. There are overpressure valves on both sides of the gate to avert a catastrophe during the procedure.

Glass Vessel

Figure 6 shows several views of the Tormac vacuum vessel. It is made of pyrex, epoxied together with Stycast 1266 resin. Ports were ground to fit, prior to gluing and care taken to minimize the area of epoxy exposed to vacuum.

The sides and inner cylinder are 1/2" thick, the outside cylinder 1/4". There is a 1 1/2" diameter pumping port on one of the sides. A fitting in the stainless vacuum manifold allows this port to be used for diagnostics as well. There

are nine additional ports for diagnostics, each approximately 1/2" in diameter. Eight of these are specifically for Thomson scattering, three pairs of laser ports set at different major radii and two collection ports set into the outer cylinder at different "Z" values. These ports can of course be used for other purposes, visible or ultraviolet spectroscopy, x-ray probes, magnetic or electric pickups, pressure probes, for example. The viewing ports are two piece taper joints and can be easily removed to change from one diagnostic to another. The laser ports are epoxied onto the vessel and compression fittings serve to connect windows or probes to them.

A half inch gap between the winding and vessel allows measurement of visible light emission to be made almost anywhere in the chamber.

The inner and outer cylinder can easily support the load under vacuum. There was some concern about the strength of the sides and of the epoxy seals. For an annulus supported on its inner and outer radius the stress (see figure 16)

$$S_r = \frac{6KWa^2}{t^2}$$

$S_r$ = maximum radial stress
W = loading
a = radius
t = thickness

For uniform loading and an inner radius one third the outer (our case) K = .055. Thus $S_r$ = 1600 PSI. For tempered glass safe design is taken to 1000 to 5000 PSI. We exceed the former figure but it is a very conservative one.

Control - Timing and Triggering

For a normal shot, many separate operations must be performed in sequence. Two separate units control the timing. One on a slow time scale, closes the gate valve, fills the vessel with gas, then passes control to a fast timing chassis. After the shot the gate valve is opened to pump out the vessel. The intervals are set by timing relays.

A digital delay circuit performs the fast timing. It consists of ten channels, each counting down off a common clock. Delays are adjustable from .1 to 1000 microseconds and are accurate to .1 microsecond. The output of the delay circuit initiates various electronic sequences, discharging capacitor banks, firing the ruby laser, triggering scopes or the computer.

Ignitrons are used to switch the large capacitor banks. Ignitron firing circuits step up the voltage and current of the timing pulse to levels capable of triggering ignitrons (1500 V @ 200 A). These circuits employ SCR's or hydrogen thyratrons to control the high voltage. Transformers are used to isolate the triggering circuit from the very high voltage, low impedance banks. Diode strings protect the ignitron trigger electrode. There is a 1 to 8 fan out to fire the series ignitrons of the cusp bank. This insures that all eight receive triggers simultaneously and reliably. A similar fan out fires the crowbar ignitrons.

Data Collection

Data collected from the experiment is almost exclusively in the form of electrical waveforms. Some of these waveforms are recorded with oscilloscopes and cameras, but, with 20 to 30 separate traces to be taken on each shot, using scopes becomes impractical. Moreover, analyzing data from oscilloscope pictures is tedious and inexact. Digitizing the waveforms is an attactive alternative but the bandwidth needed, up to 4 MHz, and the large number of channels makes direct digitizing prohibitively expensive.

To solve this problem J. Coonrod has developed a data collection scheme which takes advantage of the low repetition rate inherent in the experiment, 100 microseconds on, several minutes off.[43] Data is collected in parallel and stored in analog charge transfer devices (Reticon SAM 128). After each shot the channels are read out serially at a slow rate (~ 100 kHz) and digitized. The read out sequence is controlled by a PDP 11-34 computer. The data is displayed on graphics terminals for analysis on the spot or stored on disc or tape. Up to 32 channels of data at rates from 1 to 5 MHz can be collected. Resolution is about 1%. Figure 18 shows a rough schematic of the system.

Electrical Safety

Due to the danger posed by the high voltage capacitors used in the experiment, great care is taken to reduce the

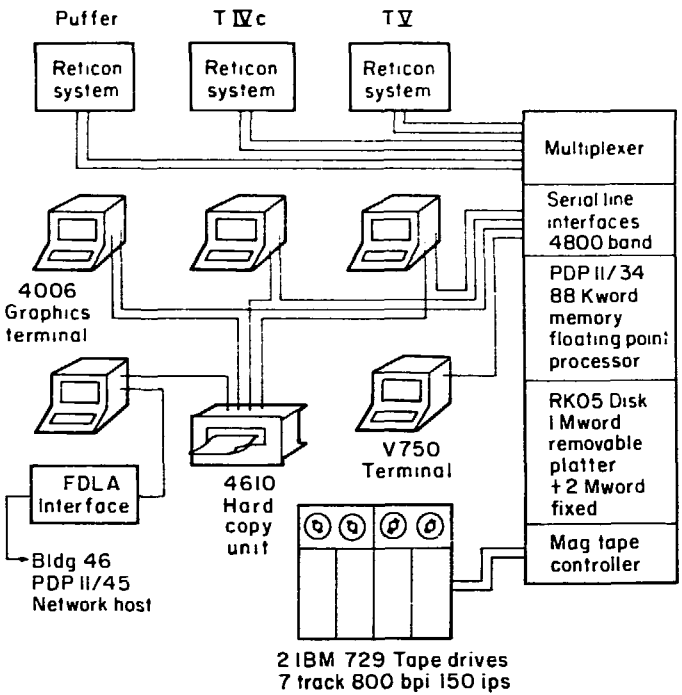
Tormac data acquisition computer system
Puffer
T IVc
T V
Reticon system
Reticon system
Reticon system
Multiplexer
Serial line interfaces 4800 band
PDP 11/34 88 Kword memory floating point processor
RK05 Disk 1 Mword removable platter +2 Mword fixed
Mag tape controller
4006 Graphics terminal
FDLA Interface
Bldg 46 PDP 11/45 Network host
4610 Hard copy unit
V750 Terminal
2 IBM 729 Tape drives 7 track 800 bpi 150 ips
XBL 789-2225

Fig. 18

possible hazard. The equipment was built to conform to LBL rules summarized in UCID 3937. The experiment is contained in a screen room with wire mesh walls and a conducting floor. Doors to the cage are interlocked preventing operation of the experiment unless they are closed and locked. Opening a door removes power from all high voltage equipment and soft grounds the capacitor banks. To render the equipment safe, two people must be present. The first unlocks and enters the cage and places hardgrounds across all capacitor banks. The second observes the procedure; and both must agree that the experiment is safe before work on it begins.

A flashing red light above the cage indicates that the experiment is energized. There is a crash off switch located by either door and well marked. Finally, all personnel are trained in CPR, in case of an accident.

## APPENDIX B THOMSON SCATTERING

### Introduction and Theory

Laser scattering, as a method for measuring plasma electron temperature, has been used since the early 1960's. It offers many advantages; the measurements are generally unambiguous, unperturbing, have good spatial and temporal resolution, and can be made over a wide range of plasma parameters. It has by now become a routine, although difficult, diagnostic.[47-49]

Careful derivations are given by many authors.[50-53] However, the basic physics of the technique can be understood in the following manner. (See Fig.19 for geometry.) The electric field of an electromagnetic wave will accelerate a free electron,

$$\dot{v} = E_o \frac{e}{m_e} \qquad E_o = \text{amplitude of EM wave}$$

The electron will radiate according to the classical formula

$$E_s^2 = \frac{e^2 \dot{v}^2}{R^2 c^4} = \frac{e^4 E_o^2}{R^2 m_e^2 c^4}$$

where $E_s$ = amplitude of scattered field

R = distance from electron to observer

Integrating over all angles we find the scattered power

$$P_s = \sigma E_o^2 \quad \text{where } \sigma = \left(\frac{e^2}{m_e c^2}\right)^2 = r_o^2$$

More careful calculations give the total cross section for Thomson scattering.

THE INPUT WAVE VECTOR IS $\bar{K}_o$, THE SCATTERED WAVE VECTOR IS $\bar{K}_s$, THE SCATTERING ANGLE IS $\theta$, $\bar{V}$ IS THE VELOCITY OF THE SCATTERING ELECTRON AND $\bar{K}_f$ IS $\bar{K}_s - \bar{K}_o$.

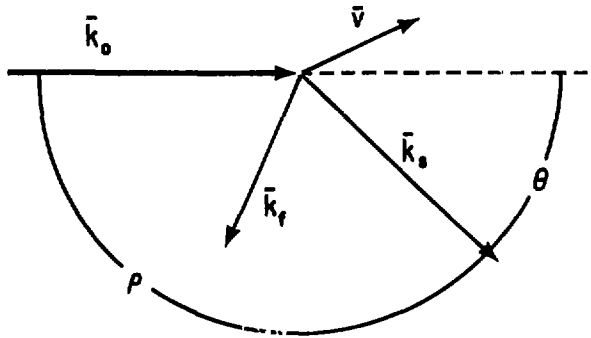


Geometry for scattering theory

XBL 789-2205

Fig. 19

$$\sigma_T = r_o^2 = 6.6 \times 10^{-25} \text{ cm}^2$$

If there are many electrons in the scattering volume, wavefronts originating at different electrons will interfere constructively or destructively. The net scattering, in this case, is due to fluctuations in the electron density. This can be seen as follows. We divide the scattering region into many cells, small enough so that the phase, $\psi_j$ of scattered light arriving at an observer from a cell, is constant. The average number of electrons in each cell is N, the number in cell j is $N_j \equiv \bar{N} + \delta N_j$. The electric field from scattering of electrons of an individual cell is

$$E_j \sim N_j e^{-i\psi_j} = (\bar{N} + \delta N_j) e^{-i\psi_j}$$

The total scattered field is

$$E_s \sim \sum_j (\bar{N} + \delta N_j) e^{-i\psi_j}$$

If the total number of cells is large the term $\sum \bar{N} e^{-i\psi_j} \to 0$, thus

$$E_s \sim \sum_j \delta N_j e^{-i\psi_j}$$

The scattered intensity

$$I_s = E_j E_k^* \sim \sum_j \sum_k \overline{\delta N_j \delta N_k} \cdot e^{-i(\psi_j - \psi_k)}$$

For the case of no correlations between cells only terms with $j = k$ remain, giving

$$I_s \sim \sum_j \overline{\delta N_j^2} = \sum_j N_j = N$$

where N is the total number of electrons.

The formal result for the differential cross section is

$$\frac{d^2\sigma}{d\omega d\Omega} = r_o^2 \sin^2\theta S(k,\omega)$$

where $S(k,\omega) = \frac{1}{2\pi V} \int d^3a \int dt \langle n(r,t)n^*(r+a,t+\tau)\rangle e^{i(ka-w\tau)}$

In general calculation S(k,w) is difficult. Results under many conditions are in the standard references.[54,55] We note that many plasma parameters can affect the form of S(k,w); electron or ion temperatures, fluid velocity, magnetic fields, collisions and others.

We see that the scattering will be incoherent if there are no correlations over cells roughly one wavelength in size. Furthermore, we can expect no correlations on a scale smaller than a Debye length. Quantitatively it can be shown that the condition for incoherent scattering is $\alpha << 1$ where

$$\alpha \equiv \frac{1}{k\lambda_D} = \frac{\lambda_o}{4\pi\lambda_D \sin\theta/2}$$

This condition is easier to meet for large angles. This is the regime we want to be in to measure electron temperatures.

If an electron is moving with respect to the source of the electromagnetic radiation and the observer (both in the lab frame) one measures a Doppler shift in the scattered light. Light scattered off a collection of electrons should give information on the velocity distribution of the electrons. From Fig. 19 and some simple geometric arguments we can see

that the component of electron velocity that lies along $k_f$ will give rise to a net doppler shift

$$\Delta\omega = k_f \cdot v$$

$$k_f = 2k_o \sin \theta/2 \quad \text{for } |k_o| \cong |k_s|$$

For a maxwellian distribution of electrons

$$f(v) = \frac{n_e}{\sqrt{T_e}} e^{-\frac{1}{2}\frac{mv^2}{T_e}}$$

(We take a one-dimensional distribution along $k_f$.)

$$S(\Delta\omega) = \frac{n_e}{\sqrt{T_e}} e^{-\left(\frac{mc^2\Delta\omega^2}{8\omega_o^2 T_e \sin^2\theta/2}\right)}$$

For the parameters of present experiment we can write this explicitly in the form

$$S(\Delta\lambda) = \frac{n_e}{\sqrt{T_e}} e^{-\left(\frac{\Delta\lambda}{19.46}\right)^2}$$

$\Delta\lambda$ in Angstroms

$T_e$ in electron volts

The shape of the scattered spectrum can be used to determine $n_e$ and $T_e$. See Figures 20 and 21.

Perturbations Induced by the Source

Because of the very small cross section for Thomson scattering, an intense source must be used to provide adequate signal. For the method to be useful as a plasma diagnostic we must demonstrate that the source (usually a high powered laser) will not seriously disturb the plasma.

For $\omega_o >> \omega_p$ (ordinarily the case) the most important

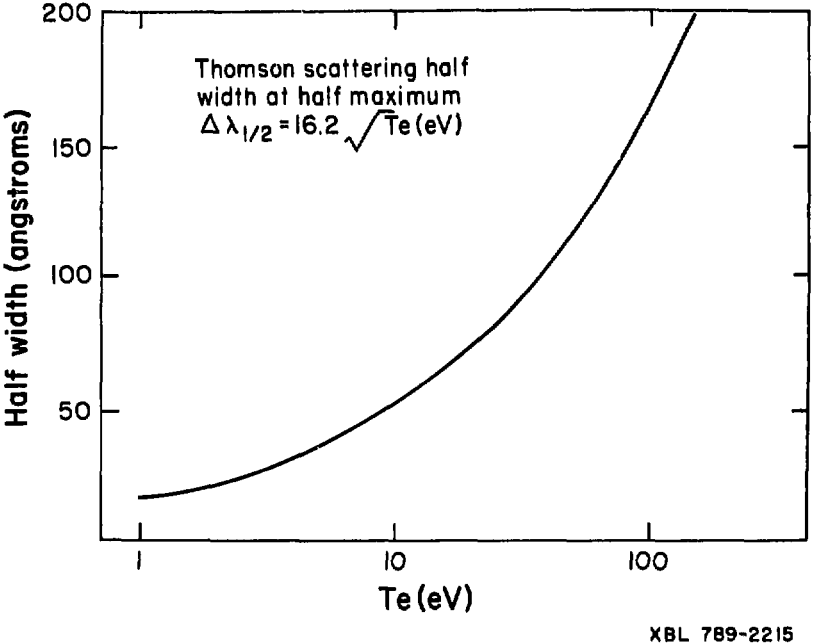


HALF WIDTH AT HALF MAXIMUM OF THE THOMSON SCATTERING ELECTRON FEATURE PLOTTED VS ELECTRON TEMPERATURE.

Fig. 20

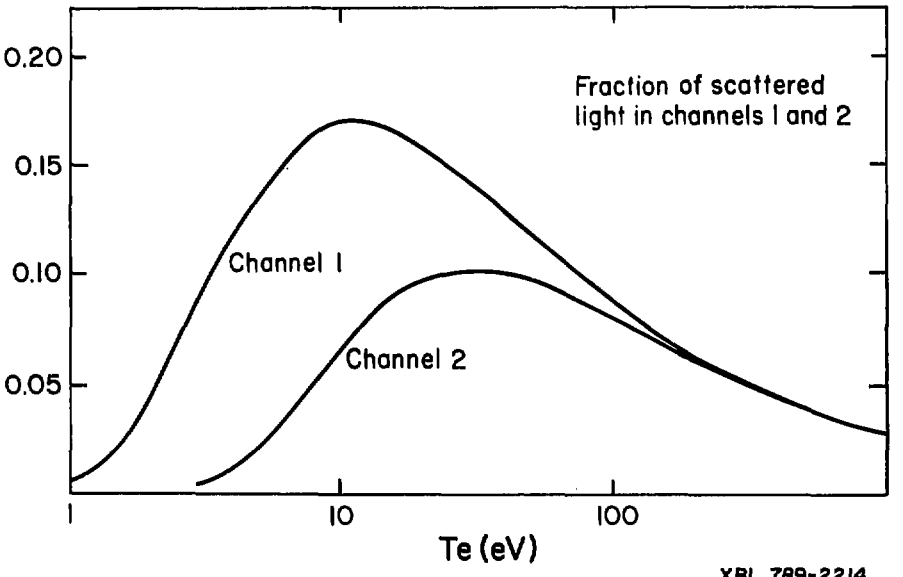


XBL 789-2214

FRACTION OF SCATTERED LIGHT WITHIN THE SPECTRAL RANGE OF POLYCHROMATOR CHANNELS 1 AND 2 PLOTTED VS ELECTRON TEMPERATURE. FOR TIMPERATURES LESS THAN 10 eV, SCATTERING INTO CHANNELS 3 AND ABOVE IS INSIGNIFICANT.

Fig. 21

perturbation will be from heating of electrons by the process of inverse Bremsstrahlung.[56,57] The rise in temperature

$$\frac{\Delta T_e}{T_e} = 1.4\times10^{25}\ \frac{n_i z^2}{(kT_e)^{3/2}}\ \frac{g_{ff}}{\nu_o^3}\ \left(1 - e^{-\frac{h\nu_o}{kT_e}}\right) I_o$$

where $g_{ff}$ is the Gaunt factor for free free transitions

$\nu_o$ is the source frequency

$I_o$ is the incident intensity (Watts/cm$^2$)

For our parameters (and $I_o$ = 10j/cm$^2$)

$$\frac{\Delta T_e}{T_e} \approx 3 \times 10^{-17}\ \frac{n_e}{(T_e)^{5/2}} \quad (T_e \text{ in eV})$$

This is plotted in fig 22 and is quite small. The above expression assumes that thermal conductivity is low enough so that heat absorbed during a laser pulse is not carried away from the scattering region. This condition is generally satisfied, and will heat conduction would lead to a smaller temperature rise in any event.

An intense laser beam can ionize and excite neutral atoms. While the cross section for these processes are small, the number of photons is very large. However, the overall effect on plasma conditions is negligible in all but very cold plasmas.

Practical Considerations

As we have seen, the cross section for Thomson scattering is very small.

$\sigma_T \sim 10^{-24}$ cm; the total scattered power $P_s$ per cubic centimeter is

THE FRACTIONAL RISE IN ELECTRON TEMPERATURE DUE TO ABSORBTION OF RUBY LASER LIGHT IS PLOTTED VS ELECTRON TEMPERATURE. THE INCIDENT ENERGY DENSITY IS TAKEN TO BE 10 J/cm$^2$.

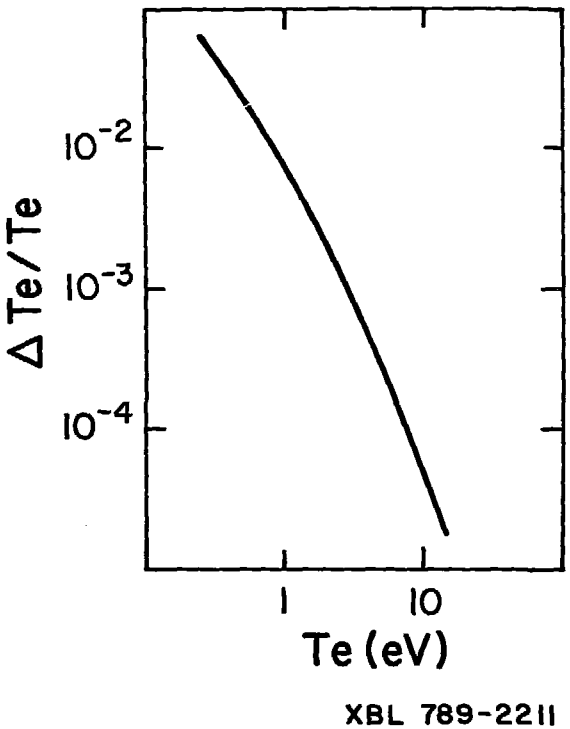


Fig. 22

$$P_s = n\sigma_T I_o$$

As an example choose $n = 5 \times 10^{15}$ (typical $T_{IV}$). Then

$$P_s = 5 \times 10^{-9} I_o$$

and of course we can expect to collect only a fraction of the total power. This puts two broad requirements on a system designed to measure electron temperature in this manner.

1. We must collect a sufficient number of scattered photons to obtain a statistically significant spectrum. This requires a strong source (a laser) and the collection of as many of the scattered photons as possible.
2. We must collect as few photons as possible which are not from Thomson scattering.

There are two sources of photons which we need to minimize

a. Light from the laser which has scattered off of imperfections in the optical train (scratches, dust, subsurface imperfections for example) and which is unshifted in frequency. This is potentially a serious problem because of the enormous intensity of the incident beam. However, with care taken in the design and execution of the experiment stray light levels can be made very small.
b. Light from the plasma. We cannot avoid collecting plasma light but by using short, intense laser pulses and limiting our observations in time and space we can reduce the plasma light collected. Nevertheless it is a major source of

noise in the measurement, often the dominant source.

Figure 23 is a schematic of the scattering apparatus. We will now consider the design of its components bearing in mind the requirements listed alone. In addition; the ports, our access to the plasma, are of fixed size and location.

The main parts of the system are:

1. a Q switched ruby laser
2. input optics to steer the beam through the plasma
3. the plasma, a target for the scattering
4. collection optics
5. a spectrometer to disperse scattered light
6. electronics to detect and record scattered light

The Laser

Before we can design the optical system for putting the laser beam through the plasma vessel, we must know the characteristics of the beam.

The ruby laser used in these experiments is made by Apollo (Model 5). It has a 15 cm long rod, 1.5 cm in diameter, pumped by a helical flash lamp with a 90 cm arc length. Overall cavity length is 60 cm. The Q switching is accomplished by a Pockels cell in a half wave, pulse on mode. In this mode the Pockels cell is placed in the cavity between the ruby rod and a pile of plates polarizer. (See Figure 24)

The polarizer is oriented perpendicular to the ruby c-axis (lasing occurs with polarization along this axis) and spoils the

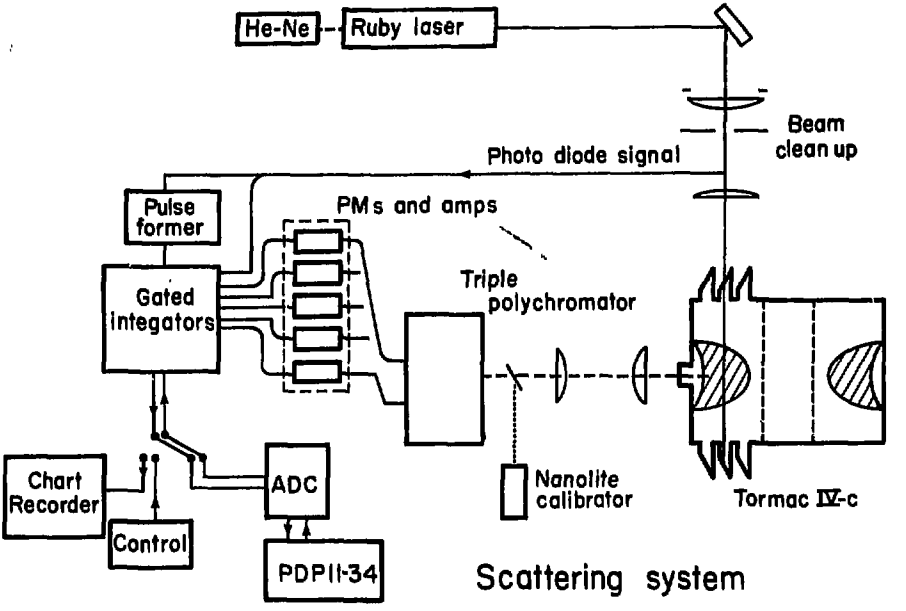
He-Ne
Ruby laser
Beam clean up
Photo diode signal
Pulse former
PMs and amps
Gated integators
Triple polychromator
Chart Recorder
Control
ADC
PDP11-34
Nanolite calibrator
Tormac IV-c
Scattering system
XBL 789-2208

Fig. 23

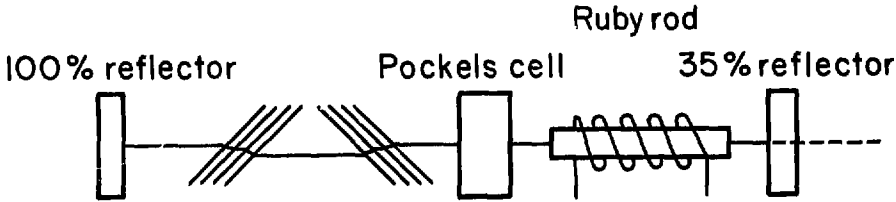


Ruby laser

XBL 789-2216

Fig. 24

cavity Q. When half wave voltage is applied to the Pockels cell light polarized parallel to the c axis is rotated by the cell and passes through the polarizer without reflection. The voltage is applied to the Pockels cell at the peak of the flashlamp induced population inversion and thus rises within a few nanoseconds. The result is a single large pulse, lasting for 25 nanoseconds. Pulse energy is 1 to 4 joules depending on voltage applied to the flashlamps (see Figure 25).

The optimum time for firing the Pockels cell is determined by plotting pulse energy vs. Pockels cell timing (see Figure 25). Once determined, the time delay between flashlamp firing and Q switching is fixed.

The front and rear reflectors of the laser cavity must be carefully alligned. This is accomplished by incorporating the laser elements in a Michelson interferometer, using a He-Ne laser (incorporated into the system for aligning the scattering system). Fringes are easily obtained and by careful adjustment the front and rear mirrors can be made parallel to about a quarter wave or about 3 seconds of arc. The Pockels cell is aligned by centering the Pockels cell pattern (obtained by placing crossed polarizers on either side of the cell and illuminating with white light) on the optic axis.

The laser head (rod and flashlamps) is cooled using a closed system of filtered, deionized, distilled water which is heat exchanged with water from a local cooling tower. The laser will operate at rates up to 3 or 4 pulses per minute.

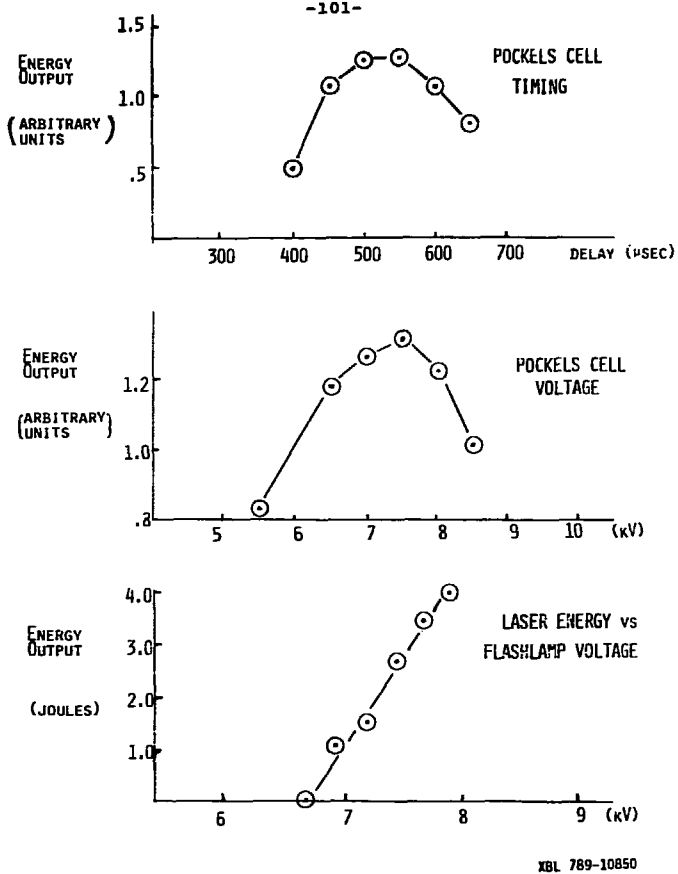
ENERGY OUTPUT
(ARBITRARY UNITS)
1.5
1.0
.5
300
400
500
600
700
DELAY (μSEC)
POCKELS CELL TIMING
ENERGY OUTPUT
(ARBITRARY UNITS)
1.2
1.0
.8
5
6
7
8
9
10
(kV)
POCKELS CELL VOLTAGE
ENERGY OUTPUT
(JOULES)
4.0
3.0
2.0
1.0
6
7
8
9
(kV)
LASER ENERGY vs FLASHLAMP VOLTAGE
XBL 789-10850

Fig. 25

The beam profile was measured by a method developed by Rory Niland and the author (similar schemes apparently are in common use). The laser beam is focused with a weak lens, through a glass plate set at approximately 45° to the beam (see Figure 26) and onto a sheet of exposed polaroid film. At each interface, part of the beam is transmitted and part is reflected. One obtains beams of varying intensitites (from $8 \times 10^{-1}$ to $1 \times 10^{-4}$ of the original) all focused on the film. The sizes of the burn marks are measured and plotted against the inverse of the intensity of the beam making the mark. Converting to angular coordinates

$$\theta = x/f$$

x = size of burn mark

f = focal length of lens

we have a plot of power/steradian vs radians (see Figure 27). For the Apollo laser the half power angle is 2.5 mR. We can call this the laser divergence. We will use the complete profile (particularly the peak, on axis, intensity) in subsequent calculations.

The procedure is repeated a short distance in front of the laser and with no lens. One obtains a plot of power/$cm^2$ vs r across the beam. This plot is essentially flat.

A quick check of laser polarization using a glass plate at the Brewster angle shows the beam to be highly polarized in a vertical plane.

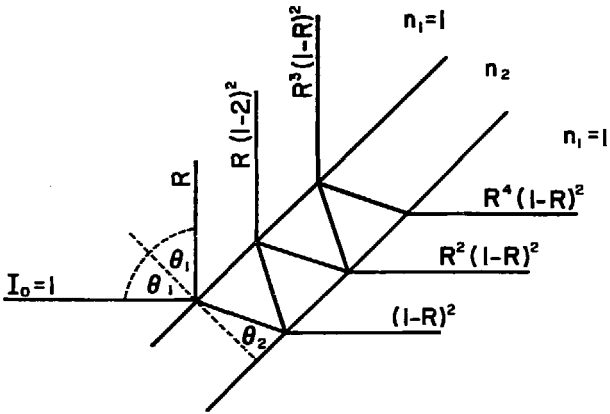


$$R = R_s = \frac{\sin^2(\theta_1 - \theta_2)}{\sin^2(\theta_1 + \theta_2)} \qquad \theta_2 = \sin^{-1}\left(\frac{\sin\theta_i}{n_2}\right)$$

# Intensities of multiple reflections from glass plate (s polarization)

XBL 789-2203

SCHEMATIC OF DEVICE USED FOR MEASURING INTENSITY PROFILES OF THE RUBY LASER BEAM.

Fig. 26

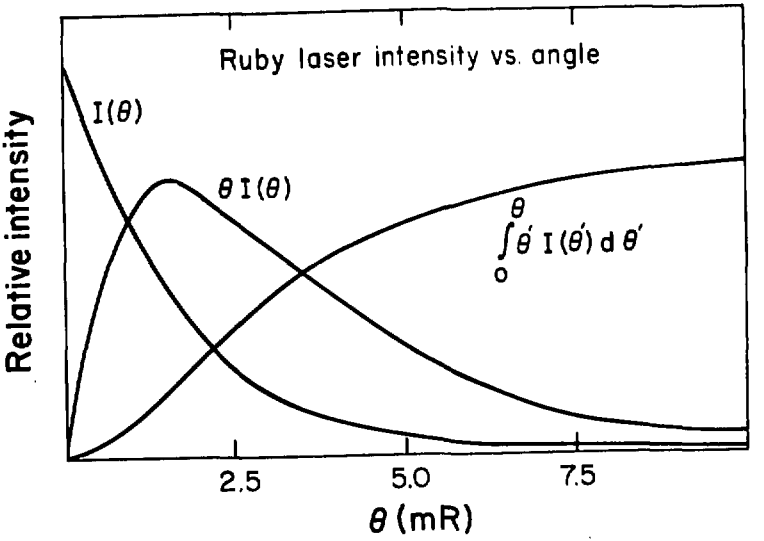


XBL 789-2212

PROFILES OF THE RUBY LASER INTENSITY VS DIVERGENCE ANGLE. $I(\theta)$ IS THE POWER EMITTED PER STERADIAN, $I(\theta)$ IS THE POWER EMITTED BETWEEN THE ANGLES 0 AND $\theta+d\theta$ AND $\int I(\theta)\, d\theta$ IS THE POWER EMITTED AT ANGLES LESS THAN $\theta$.

Fig. 27

Input Optics

There are several considerations in the design of the input optics. The beam must be put cleanly through ports in the vacuum vessel with the least amount of stray light scattered in the collection optics. The beam should be focused in the plasma to maximize the incident laser power. (For many systems it is desired to measure $T_e$ at several places along the beam, necessitating a weaker focus). The power levels on the vacuum windows must be kept below their damage threshold. We also must be able to fit the system into available space (they tend to be quite long) and it is desirable to use commercially available lenses in the construction. These considerations are, to some extent, in conflict and an attempt was made to roughly optimize the design.

Most of the power in the beam is concentrated in a small range of angles near 0°. However, a considerable amount propagates at larger angles. If unrestricted, this light would bathe the experiment in laser light. In the optical system shown in Figures 28 and 29 the combination of the two stops and the first lens restricts the range of angles which are transmitted. The second lens serves to focus the beam through the ports.

The ray transfer matrix for the system is (for U > 0)

$$M = \begin{pmatrix} 1 & U \\ 0 & 1 \end{pmatrix} \begin{pmatrix} 1 & 0 \\ -S_2 & 1 \end{pmatrix} \begin{pmatrix} 1 & D \\ 0 & 1 \end{pmatrix} \begin{pmatrix} 1 & 0 \\ -S_1 & 1 \end{pmatrix} \begin{pmatrix} 1 & Q \\ 0 & 1 \end{pmatrix}$$

multiplying

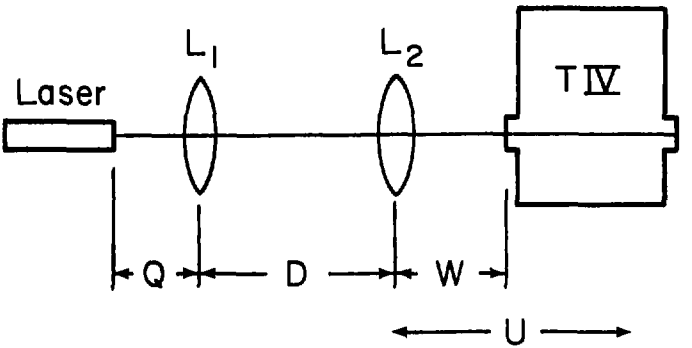


# Geometry for input optics

XBL 789-2217

GEOMETRY USED IN THE DESIGN OF THE INPUT OPTICS. TWO LENSES ARE EMPLOYED. THE FIRST IS PART OF THE BEAM CLEANUP SYSTEM; THE SECOND FOCUSES THE BEAM THROUGH THE VESSEL.

Fig. 28

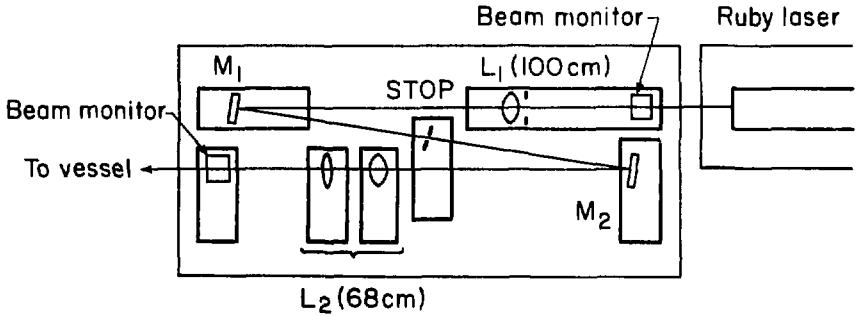


Layout for input optics

XBL 789-2218

Fig. 29

$$M = \begin{pmatrix} 1 + U(-S_1-S_2+DS_1S_2) & Q(1-DS_1-US_1(1-DS_2)-US_2) \\ & \quad + U(1-DS_2) + D \\ -S_1-S_2+DS_1S_2 & - QS_2 + (1-DS_2)(1-QS_1) \end{pmatrix}$$

where $S_1 = 1/f_1$ the power of lens 1

$S_2 = 1/f_2$ the power of lens 2

(For further explanation of the method see reference 67.)

For $-D < U < 0$

$$M = \begin{pmatrix} 1 & D+U \\ 0 & 1 \end{pmatrix} \begin{pmatrix} 1 & 0 \\ -S_1 & 1 \end{pmatrix} \begin{pmatrix} 1 & Q \\ 0 & 1 \end{pmatrix}$$

$$= \begin{pmatrix} 1-S_1(D+U) & Q+(D+U)(1-QS_1) \\ -S_1 & 1-QS_1 \end{pmatrix}$$

A computer code (written by R. Niland) traced a large collection of rays (10,000 to 50,000) through the optical system. The distribution of initial positions and angles was chosen to match the measured properties of the laser beam. Parameters of the optical system ($f_1$,$f_2$,D) were then adjusted to give the best overall design. Final values were

$Q = 70$ cm

$D = 215$ cm

$W = 100$ cm

$Q+D+W = 385$ cm

$f_1 = 100$ cm

$f_2 = 68.5$ cm

stop 1 = 1.5 cm in diameter

stop 2 = .5 cm in diameter

There was no lens available with a focal length of 68.5 cm. However, with 2 weaker lenses spaced a distance d apart the same effect can be obtained.


We are given $f_T = 1/S_T = 68.5$ cm.

To determine A and B set

$$\begin{pmatrix} 1 & 0 \\ -S_2 & 1 \end{pmatrix}\begin{pmatrix} 1 & d \\ 0 & 1 \end{pmatrix}\begin{pmatrix} 1 & 0 \\ -S_1 & 1 \end{pmatrix} = \begin{pmatrix} 1 & B \\ 0 & 1 \end{pmatrix}\begin{pmatrix} 1 & 0 \\ -S_T & 1 \end{pmatrix}\begin{pmatrix} 1 & A \\ 0 & 1 \end{pmatrix}$$

$$\begin{pmatrix} 1-dS_1 & d \\ -S_1-S_2+dS_1S_2 & 1-dS_2 \end{pmatrix} = \begin{pmatrix} 1-BS_T & A+B-ABS_T \\ -S_T & 1-AS_T \end{pmatrix}$$

so $S_T = S_1+S_2-dS_1S_2$

$A = dS_2/S_T$

$B = dS_1/S_T$

If we choose $f_1 = 100$ cm, $f_2 = 200$ cm we find

$d = 8.0$ cm

$A = 2.95$ cm

$B = 5.5$ cm

and we note A+B = 8.25 cm so A+B-D = .25 cm << 68.5. Figure 29 shows the input system in more detail. The optical path

is folded to accomodate the nearly 4 meter length into the TORMAC IV screen cage. The mirrors also provide a convenient means for steering the beam through the ports. $M_1$ is adjusted to put the beam on $M_2$ at a spot colinear with the center of the two ports. $M_2$ is then set at an angle to put the beam through them. The mirrors are 2 inches in diameter with hard dielectric coatings, flat to $\lambda/10$. The mounts have micrometer adjustments for both angles.

The lens mounts have micrometer adjustment for translation in the two directions perpendicular to the beam, as does stop 2. Stop 2 is made from 1" round brass stock machined to leave a .5 cm aperture with very sharp edges.

There are two beam monitors. They consist of a thin sheet of glass set at 45° to the beam and reflect about 1% of the incident light onto a pair of opal glass diffusers and then to a hp 5082-4220 Pin diode (response time 1 → 2 nsec). The diffusers keep the monitor from being overly sensitive to the beam profile which will vary a bit from shot to shot. At high light levels the diode will saturate and distort the waveform. Output should be kept below 20 mA with these devices.

The ports are of quartz, set at the Brewster angle for 6943. Efforts were made to keep them clean and free of scratches. A beam dump of Corning CS 4-72 dye glass, set at the Brewster angle completes the input system. CS 4-72 has an an attenuation length of about .6 mm at 6943 and can absorb large energies without damage.

It is worthwhile at this point to say a few words about damage to optical components from high powered lasers. Values for damage thresholds, given in the literature, vary over a wide range.[58-60] For visible frequencies and pulse lengths of 10 to 30 nanoseconds values from 20 MW to over 1 GW are cited. This is due in part to the tolerance of different materials, but of greater importance is the condition of the optical surface in determining the susceptibility of a particular material to damage. Even if care is taken to keep dirt and dust off a polished surface; small, sometimes microscopic, defects and cracks in surface or subsurface layers can greatly enhance absorption and damage. Superpolishing techniques are sometimes used to remove these defects. The technique is similar to ordinary optical grinding and polishing but employs many small steps, and carried out for longer periods. It is, of course, quite expensive.

Dielectric coatings can tolerate incident intensities of around 5 joules/$cm^2$ delivered in a 20 nanosecond pulse. Coatings will vary and batches with particularly good or bad characteristics are not uncommon. Partially reflecting mirrors are the most fragile, followed by fully reflecting and nonreflective coatings.

Cemented doublets can stand only very low power and should not be used in the main beam path. Lenses with short focal lengths are susceptible to internal damage. In these, multiple reflections can lead to a sharp focus inside the lens.

All optics in the input system are held on a table made of 1" thick aluminum supported by concrete pillars. Wood and rubber spacers keep the entire assembly stable and relatively free of vibration. Optical rails are mounted on the aluminum table and the individual optical elements and their mounts are placed on the rails. The elements are moved along the rails to shift the beam between the 3 sets of ports available on the TORMAC IV-c experiment. The overall system is easy to adjust and align, flexible and quite stable.

Collection Optics

The collection optics must gather as much of the scattered light and as little of the plasma light as possible. In TORMAC IV a compromise had to be made. The polychromator used had been designed and built for TORMAC V and was matched to that geometry. TORMAC IV can collect light over a layer solid angle and would overfill the polychromator. However, scattering signal to noise on TORMAC V was quite good and would be as good on TORMAC IV. Instead of building a new polychromator to fully utilize the new geometry, the angle of acceptance was reduced.

The collection geometry, given in Figure 30, employs two lenses. There are five degrees of freedom in the design, the three distances and the focal lengths of the lenses. To optimize the system we will require the target to be imaged onto the polychromator slit and the port onto the grating.

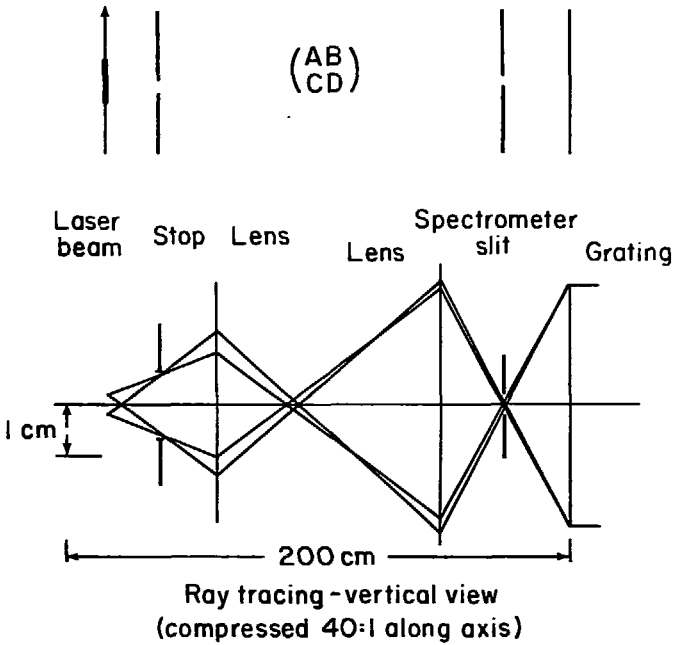


XBL 789-2221

GEOMETRY FOR COLLECTION OPTICS CALCULATIONS AND SAMPLE RAYS TRACED IN THE FINISHED SYSTEM. THE SCALE IS GREATLY COMPRESSED ALONG THE OPTICAL AXIS.

Fig. 30

The magnification must be set so that the target image fills the slit and the port image fills the grating. We are left with one degree of freedom. For convenience we can choose $f_1 = f_2$. If we allow the system to slightly underfill the grating (we are nowhere near the diffraction limitations in the spectrometer) we can use readily available lenses.

Referring again to figure 30, we begin the calculations. The transfer matrix from target to slit is

$$\begin{pmatrix} A & B \\ C & D \end{pmatrix} \begin{pmatrix} 1 & 220 \\ 0 & 1 \end{pmatrix} = \begin{pmatrix} A & 220A+B \\ C & 220C+D \end{pmatrix}$$

If the target is imaged onto the slit $220A+B = 0$ and $A = m$ (the magnification) thus $B = -220\ m$ (distances in cm). The matrix from stop to grating is

$$\begin{pmatrix} 1 & 26.0 \\ 0 & 1 \end{pmatrix} \begin{pmatrix} A & B \\ C & D \end{pmatrix} = \begin{pmatrix} A+26C & B+26D \\ C & D \end{pmatrix}$$

to image the stop on the grating

$$B + 26.0D = 0$$

$$D = \frac{-B}{26.0} = \frac{22.0}{26.0}\ m$$

$$m' = A + 26.0C$$

Since $AD - BC = 1$

$$C = AD-1/B = \frac{22.0m^2}{26.0} - 1/-220m$$

$$C = \frac{1}{220m} - \frac{m}{26.0}$$

and

$$\begin{pmatrix} A & B \\ C & D \end{pmatrix} = \begin{pmatrix} m & -22.0m \\ 1/22.0m - m/26.0 & 22.0m/26.0 \end{pmatrix}$$

for a two lens system

$$|\leftarrow d_3 \rightarrow ()\leftarrow d_2 \rightarrow ()\leftarrow d_1 \rightarrow |$$

$$\begin{pmatrix} A & B \\ C & D \end{pmatrix} = \begin{pmatrix} 1 & d_1 \\ 0 & 1 \end{pmatrix} \begin{pmatrix} 1 & 0 \\ -S_1 & 1 \end{pmatrix} \begin{pmatrix} 1 & d_2 \\ 0 & 1 \end{pmatrix} \begin{pmatrix} 1 & 0 \\ -S_2 & 1 \end{pmatrix} \begin{pmatrix} 1 & d_3 \\ 0 & 1 \end{pmatrix}$$

It can be shown (with $S_1 = S_2 = S = 1/f$)

$$d_1 = A/C + S_2/CS_1 + 1/S_2 = (1+A)/C + f$$

$$d_2 = C/S_1S_2 + 1/S_1 + 1/S_2 = Cf^2 + 2f$$

$$d_3 = D/C + S_1/CS_2 + 1/S_2 = (1+D)/C+f$$

$$L = d_1 + d_2 + d_3 = \frac{2+A+D}{C} + 4f + Cf^2$$

using the previous result

$$d_1 = \frac{1 + m}{(\frac{1}{22.0m} - \frac{m}{26.0})} + f$$

$$d_2 = (\frac{1}{22.0m} - \frac{m}{26.0}) \quad f^2 + 2f$$

$$d_3 = \frac{(1 + \frac{22.0}{26.0} m)}{(\frac{1}{22.0m} - \frac{m}{26.0})} + f$$

Our input system puts most of the beam intensity into a cylinder 4 to 5 mm in diameter. The polychromator slit is 1 mm wide so we will choose m = 1/4. By trial and error we find that 15.0 cm is a good choice for f. With these values we find

$d_1$ = 18.2 cm

$d_2$ = 117.7 cm

$d_3$ = 17.8 cm

L = 1538 cm

m' = 5

The port is slightly under 1 cm so the image at the grating is fairly well matched to the 5 x 5 cm ruled area. Sample rays are traced in figure 30. (Note that the lenses employed are f/3 and are almost filled.)

Polychromator

It is standard practice in scattering experiments to include a good viewing dump in the apparatus. The dump would subtend the entire viewing angle and be non-reflective. Stacks of razor blades are often used. The Tormac IV geometry makes it impossible to reduce stray light by this means, thus another method must be employed.

Siemon, facing a similar problem on Scyllac, used a three stage polychromator based on the varoilluminator.[61,62] The

device has the property of rejecting, to a very high degree, light outside of a specified wavelength range. Stray light is recognized and eliminated by its spectral characteristics, rather than through geometry.

Figure 31 shows the triple grating polychromator, designed by W.I.B. Smith, used on TORMAC.[63] The three stages respectively disperse, recombine and redisperse incident light. The stages are identical in optics and construction, having 2" square gratings with 1200 grooves per mm and 26.0 cm focal length collimation lenses. Linear dispersion in the instrument is 30A/mm. Slit 2 is wide allowing the desired range of wavelengths ( ~ 300A) through but blocking 6943. The second grating directs remaining stray light away from the narrow slit 3. The third stage is a duplicate of the first and reduces stray light still farther. The result is an overall rejection which is the product of the 3 stages, $10^3$ to $10^4$ per stage, for a net rejection of $10^9$ to $10^{12}$. By comparison a polychromator with three dispersive stages in succession would have an overall rejection that was only the sum of the three.

The polychromator has a measured transmission of 33% for light polarized perpendicular to the rulings (the scattered light has this polarization) and less than 2% for parallel light. This will serve to improve S/N by reducing plasma light, which is unpolarized.

The polychromator output is focused onto a 1 cm square

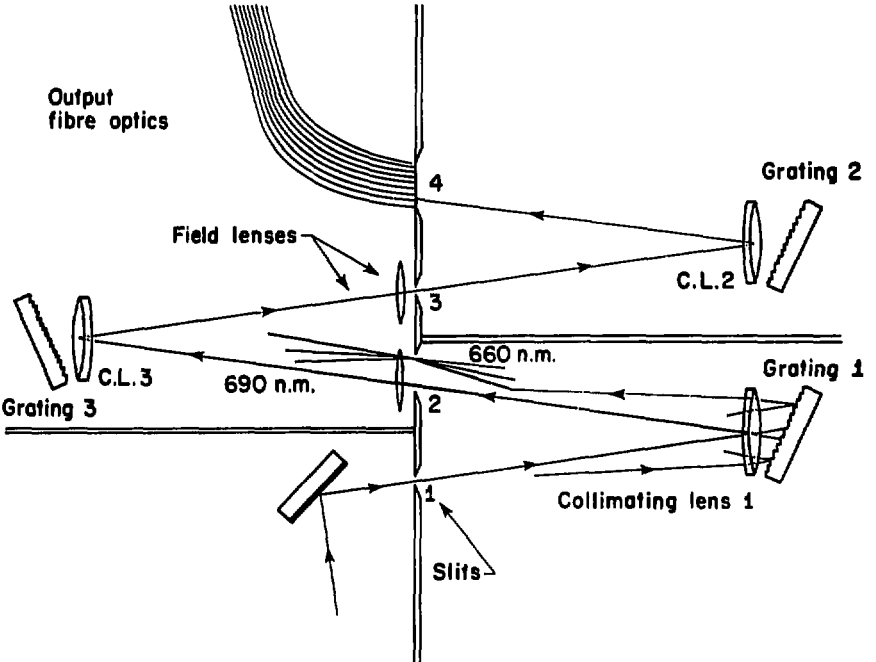


XBL 767 3168

Fig. 31

close packed array of plastic light fibers. There are ten channels, each 1 mm wide (30 A). The fibers are 6 ft long, polished at both ends. Those from each channel are bundled together in black PVC tubing and directed to a set of photomultipliers; cross talk between channels is extremely low. The fiber bundle reduces the light by about 50%, so overall instrument transmission is approximately 15%.

The instrumental rejection was measured and found to be more than $2 \times 10^{10}$ for all channels. This figure has the instrumental throughput folded in and represents the reduction of stray light relative to signal. This rejection figure was more than adequate; no stray light was seen in any TORMAC IV measurements.

Electronics

The photomultiplier used to detect the scattered signals are RCA 4836. These are small end-on tubes with extended red photocathodes (ERMA 11). The recommended voltage dividing network was used and the anode connected to a 1000 Ω load. With 3pf stray capacitance the tube should have time response of 3 nanoseconds. Current gain vs voltage was measured for all tubes and was found to be between 1 and $5 \times 10^5$ at 1500 V, our nominal operating voltage. The output were fed to a fast slewing voltage follower (Signetics LH0063), mounted physically near the photomultiplier base. The follower has unity gain, response time of a few nanoseconds and is capable of

driving a 50 Ω load. To test the photomultiplier amplifier combination a Tecktronix 110 pulse was used to drive an XP-23 fast LED. The light pulse lasted approximately 15 nsecs. The output was recorded on a sampling scope. The overall rise time was 7 nsecs. The photomultipliers were fitted with magnetic shields and housed in an aluminum chassis.

In many plasma experiments there is a great burst of visible radiation at the onset of ionization and heating. One must ensure that photomultipliers are not temporarily blinded by this light. This can be remedied by suitable filtering in the biasing circuit. Some scattering experiments gate their photomultipliers on only after the initial transient has passed. In the present work this was not found to be necessary.

In operation there were two methods for reading scattered light signals. In the simplest, signals were fed into a pair of 585 oscilloscopes. Timing was provided by the Pockels cell pulse, suitably delayed. There were only two 585's available, thus only two channels could be viewed simultaneously. Alternately the signals fed a set of Lecroy gated integrators. (Figure 23 shows the arrangement.) The gating signals were provided by a discriminator with an eightfold fanout. It was built from Schottky TTL gates and a Signetic 549 voltage comparator, driven by a beam monitor signal. This ensured accurate and reproducible timing. Timing derived from the Pockels cell signal results in excessive jitter. The gating signal

was adjustable from 10 to 100 nsecs with very steep sides. Propagation delay through the discriminator was less than that through the photomultipliers so additional delay was added to the timing pulse by means of a length of coaxial cable. The outputs of the Lecroy channels were multiplexed. A circuit was built to interrogate the multiplexe and interface it with a chart recorder.

Signal to Noise

We can make an estimate of the signal expected in the experiment. The number of photons collected by the polychomator is

$N_{photons} = N_o n_e V_o T \Omega t_c$

$N_o$ = number of photons in laser beam

$n_e$ = electron density

V = scattering volume

$\Omega$ = solid angle of collection

$t_c$ = transmission of collection optics

The laser pulse has 2 joules of energy or $7 \times 10^{18}$ photons,

$n_e = 5 \times 10^{15}$, V = .15 $cm^3$

$\Omega = 1.5 \times 10^{-3}$, $t_c = .5$, so

$N = (7 \times 10^{18})(5 \times 10^{15})(.15)(6.6 \times 10^{-25})(1.5 \times 10^{-3})(.5)$

$= 2.6 \times 10^{6}$ photons

The transmission of the polychromator is .15, we look only on the blue side of 6943 and divide the spectrum into 5 channels.

Thus each channel sees 39,000 photons. Quantum efficiency of the tubes is about 3%. Thus a typical channel generates approximately 1200 photoelectrons. The statistical fluctuations on this number is 35. We will compare this to the expected noise from plasma light.

The main source of plasma light in this wavelength region will be Bremsstrahlung. Free-bound radiation might contribute another 25 to 50%. Since the plasma parameters which generate this radiation do not change on a fast time scale (averaged over the volume in question), the plasma light level is effectively DC. It is only the fluctuations in plasma light that contribute to noise in the experiment. The noise will be given by

$$N = \sqrt{N_s + N_p} \qquad N_s = \text{number of scattering photoelectrons}$$
$$N_p = \text{number of plasma photoelectrons}$$

In many cases $N_p >> N_s$ so

$$N \approx \sqrt{N_p}$$

for signal to noise S/N in excess of 1 we have

$$N_p >> N_s >> \sqrt{N_p}$$

The Bremsstrahlung power emitted per unit volume, solid angle and wavelength interval near 6943 is[64]

$$P_B = \frac{3.0 \times 10^{-37}\ z^4\ n_e^2\ e^{-1.79/T_e}}{T_e^{1/2}} \quad \frac{\text{Watts}}{\text{cm}^3\ \text{str A}}$$

The number of Bremsstrahlung photons

$$N_B = \frac{1.0 \times 10^{18} z^4 n_e^2 e^{-1.79/T_e}}{T_e^{1/2}} \frac{\text{Watts}}{cm^3 \text{ str A}}$$

We can estimate the plasma parameters,

$n_e = 5 \times 10^{15}$

$T_e = 5$ eV

$Z_{eff} = 1.5$

and we find

$N_B = 6 \times 10^{13}$ photons/sec. $cm^3$ str A

Further, the volume of collection is

$V = .4 \times 1.2 \times 10$ cm $= 4.8$ $cm^3$

$\Omega = (1/26)^2$str

$t = 20$ nsecs

$\Delta\lambda = 30$ A

or about 320,000 photons/channel, 160,000 with the proper polarization. With .5 transmission in the collection optics .15 in the polychometer and 3% quantum efficiency we will see 360 photoelectron/channel. Adding freebound radiation at 5 eV this becomes 540 with a standard deviation of 23.

Unfortunately, as a general rule much more continuum radiation is seen from laboratory plasmas than is calculated Tormac seems to be no exception with 10 to 100 times more

light seen than expected. Measured S/N's are around 10.

Assuming that, whatever the source of the continuum it shares the same dependence on the plasma conditions we can determine the effect of various system parameters on the important S/N figure.

Increasing laser power (assuming stray light problems have been solved) increases signal and S/N in a linear fashion. Improving the focus of the beam leaves the signal alone but decreases the collected plasma light like d = focused beam diameter. Noise then decreases like $\sqrt{d}$ and S/N like $1/\sqrt{d}$. For a homogeneous plasma S/N is independent of density since S~n, N ~ $\sqrt{n^2}$. For inhomogeneous plasmas the situation is altered of course. As $T_e$ increases, the light scattered into each channel decreases by $1/\sqrt{T_e}$. (This is simply the normalization factor for a maxwellian.) Plasma light also decreases like $1/\sqrt{T_e}$ (for $T_e$ >> 1.79 eV) thus N ~ $T_e^{-1/4}$ and S/N~ $T_e^{-1/4}$. If we increase the width of each channel to keep the signal in each constant as $T_e$ increases S/N will also remain constant. This leads to the conclusion that the highest S/N is achieved when the number of channels is the minimum necessary to obtain good spectra.

Increasing the solid angle of collection (assuming properly designed optics) increases signal and plasma light by the same factor and thus improves S/N by $\sqrt{\Omega}$ where $\Omega$ is the solid angle. For a port of diameter a, S/N ~ a. (Of course for very large solid angles the scattered spectrum will be

smeared since the halfwidth $\Delta\lambda_{1/2} \sim \sin\theta/2$ and we will be collecting from a large range of angles, $\theta$.) Losses in all subsequent optics have a similar effect. Plasma light and signal are reduced by identical factors. (The polychromator passes only plasma light of one polarization but this effect has already been taken into account.) Photomultiplier quantum efficiency enters in the same manner, $S/N \sim \sqrt{QE}$ . For very low light levels first dynode statistics might play a role in increasing noise but for most experiments this effect is negligible.

Further processing of the signal has little effect on S/N. Differentiation to remove the slowly varying component of the plasma light will reduce S/N only slightly. Integration of the signal (either with an RC network or by gating) as opposed to measuring only peak values, improves S/N and is optimum for integration times approximately equal to the laser halfwidth and decreases slowly for longer integrations. When gated integrators are used, centering the gate on the laser pulse is critical and it is advantageous to use gate times comfortably longer than the laser half width.

Calibration

There are two essential calibrations for a Thomson scattering experiment. The wavelength of each channel and their relative sensitivities must be measured. The wavelength calibration should remain fixed once the instrument is assembled,

but sensitivities of photomultipliers are known to drift and should be recalibrated frequently.

Once assembled and aligned the triple polychromator has no wavelength adjustment which might be employed in calibration. Instead, a Xenon arc lamp and a second spectrometer were used as a source of monochromatic light with variable wavelength. Its wavelength scale was checked for accuracy against known sources. The signal was small so a chopper and PAR lockin amplifier were employed. Channel profiles were mapped out and plotted. The first channel was 45 A from 6943 as planned.

A fast spark was used as the source for sensitivity calibration. Light from the spark is of very short duration, rising in 10 nsecs and falling in 20-30 nsecs. Such a source has two advantages. First, since its duration is comparable to the laser pulse, any possible difference in time response of the channels is cancelled out. More importantly, the calibration can be done in situ with essentially no change in the system configuration. This enables one to do calibrations as frequently as is necessary.

The spark spectrum was determined by comparison with a standard tungsten lamp. Because of the spark's very short duration and low repetition rate (about 1 pulse per second) the gated integrators were used to measure the signals. The spectrum is shown in Figure 32. Note that it is quite flat over the range of interest and no lines are seen. In practice

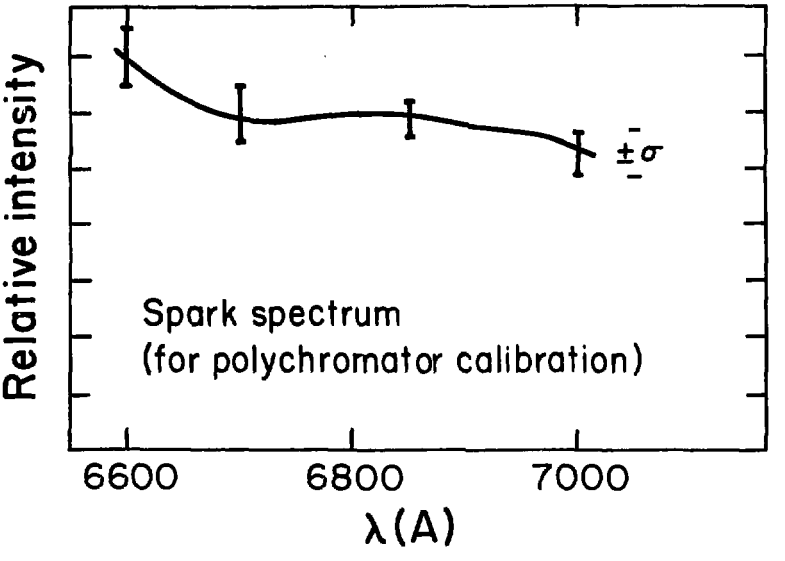


XBL 789-2210

SPECTRUM OF THE FAST SPARK USED IN POLYCHROMATOR CALIBRATION. THE SPECTRUM IS RELATIVELY FLAT AND NO LINES ARE VISIBLE IN THE SPECTRAL RANGE OF INTEREST.

Fig. 32

little change in photomultiplier response was seen, never amounting to more than 10 or 20%.

Alignment

Alignment of the input laser beam and the viewing optics is critical. At the scattering volume the beam is only 4 mm wide. The optical paths for the two optical systems are 3.5 and 1.5 meters respectively. Thus great care must be taken to ensure that they do, in fact, intersect.

The first step was to align a He-Ne laser along the axis of the ruby. This was accomplished by centering the He-Ne beam in the ruby face and on burn marks made by firing the ruby at exposed film. One mark was made close to the laser and a second several meters away. The angle between the beams was less than a third of a millaradian, a good deal less than the ruby divergence. When making burn marks close to the face of the ruby or near any optical surface; a piece of glass was interposed between the film and the optical element. This ensures that particles or smoke thrown off during the burn do not deposit on the optics. Otherwise in subsequent shots the surfaces could be damaged or broken.

With the input mirrors in the optical path but all lenses and stops removed; the He-Ne beam was sent through the centers of the scattering ports. This required tilting and moving both mirrors in increasingly smaller increments. The lenses were put in one at a time and the beam recentered with each

in place. The ruby was fired several times to recheck allignment; it should be centered on the lenses and ports. The stops were inserted. The smaller stop, at the focus of the first lens was blackened and adjusted by centering the burn mark on the aperture. Finally a burn was made at the far end of the vessel and examined for centering and any indication that the beam was glancing off metal or glass surfaces. These usually take the form of irregularities or rays in the burn pattern. Once the input is deemed to be aligned, all components were tightened firmly into place and the alignment rechecked.

The scattering volume is ordinarily inaccessible. To effect the alignment of the collection optics, the vacuum was broken and a plastic tube inserted through the laser ports. The tube contained a small mirror, set to reflect the He-Ne beam at exactly 90°. A window in the side of the tube allowed this light to be reflected through the center of the viewing port. With the collection lenses removed the He-Ne beam was sent through the polychromator, through the center of the first slit and the first grating. The lenses were installed one at a time, with the beam kept centered. A stream of dry nitrogen was used to blow dust off all optics and out of the polychromator which was then closed and sealed.

Data analysis

Data collected from either the integrators or scopes is corrected for photomultiplier response and fit to a gaussian

and $T_e$ calculated.

$$S(\lambda) \sim \frac{n_e}{\sqrt{T_e}} e^{-\left(\frac{\Delta\lambda}{19.46}\right)^2} \frac{1}{T_e}$$

$$\Delta\lambda_{1/2} = 32.4 \sqrt{Te(eV)}$$

For low temperatures (few channels) it is desirable to convolve the polychromator instrument function with the gaussian. That is one fits the function

$$\int_{-\infty}^{\infty} e^{-\left(\frac{\lambda'-\lambda}{19.46}\right)^2} I(\lambda')d\lambda$$

to the data, where $I(\lambda)$ is the instrument function. The correction is not large, however.

Density measurement

Ordinarily Rayleigh scattering can be used as an absolute calibration for one polychromator channel and allow measurement of Ne as well as $T_e$. The Rayleigh scattering is unshifted in wavelength, however, and will not be passed by the triple polychromator. If an ordinary polychromator were used, stray light would overwhelm the Rayleigh scattering signal in our case. Thus no density measurements could be made with Thomson scattering.

Optical Safety

It is worthwhile to say a few words about the dangers of

high powered lasers and necessary safety precautions. The lasers used for Thomson scattering (1-10 joules) could easily cause blindness. Reflections of specular surfaces or even diffuse reflections are serious hazards. In the present experiment the entire beam and all optics were in an interlocked enclosure and the vessel covered with dark cloth. Electrical hazards associated with the flashlamp supply were controlled in a manner described in an earlier section.

## APPENDIX C OTHER DIAGNOSTICS

### Helium Neon Interferometer

Optical interferometry, using low power CW lasers, is a powerful diagnostic. It gives a localized (in two dimensions) time resolved, non-interfering measurement of electron density. The experimental apparatus is fairly simple, inexpensive and rugged. Density measurements are not resolved along the line of sight, but are otherwise fairly unambiguous. Interfering effects, in most cases, can be shown to be small. The principle involved in the diagnostic is simple. For electromagnetic waves with frequencies much higher than any that characterize the plasma, the index of refraction depends linearly on electron density.

$$\omega_o^2 = k^2c^2 + \omega_e^2$$

$$n^2 = \frac{k^2c^2}{\omega_o^2} = 1 - \frac{\omega_e^2}{\omega_o^2}$$

n = index of refraction

$\omega_o$ = frequency of EM wave

$\omega_e$ = electron plasma-frequency

If we consider the effects of magnetic fields parallel to k,

$$n^2 = 1 - \frac{\omega_e^2}{\omega_o^2} \quad (1 - \frac{\Omega_e}{\omega_o})^{-1} \qquad \Omega_e = \text{electron gyrofrequency}$$

$\Omega_e \ll \omega_o$ for optical frequencies ($\sim 10^{15}$) for any conceivable $\Omega_e$. If the electrons are undergoing collisions at a rate $\nu_c$.

$$n^2 = 1 + \frac{\omega_e}{\omega_o} \left[1 + \frac{i\nu_c}{\omega_o}/(1 + \frac{\nu_c^2}{\omega_o^2})\right]$$

Typical cross sections for electron ion or electron atom

collisions are of the order $10^{-15}$ cm$^2$.

$$\nu_c = n_i \sigma_{ei} v_e + n_a \sigma_{ea} v_e \ll \omega_o = 10^{15}$$

even for exceedingly high densities.

So in general

$$n = 1 - \frac{\omega_e^2}{2\omega_o^2}$$

for a helium neon laser, $\lambda_o = 6528$ A, $\omega_o = 3.0 \times 10^{15}$.

$$\omega_e = 5.6 \times 10^4 \sqrt{n_e}$$

$$n - 1 = 1.77 \times 10^{-22} n_e$$

The difference in path length caused by a change in the index of refraction along one arm of an interferometer is given by,

$$\Delta L = \int (n-1) d\ell$$

The phase shift is

$$\theta_{\text{radians}} = \frac{2\pi \Delta L}{\lambda_o} = \frac{2\pi}{\lambda_o} \int n-1 \, d\ell$$

for He-Ne wavelengths

$$\theta_{\text{radians}} = 1.76 \times 10^{-17} \int n_e \, d\ell$$

$$\theta_{\text{degrees}} = 1.01 \times 10^{-15} \int n_e \, d\ell$$

for two passes through the plasma (as in a Michelson interferometer) we obtain the result

$$\int n_e \, d\ell = 4.97 \times 10^{14} \, \theta_{\text{degrees}}$$

Interference intensity depends sinusoidally on phase shift

$$I = I_o \sin\theta \qquad I_o = \text{full modulational intensity}$$

Thus the expression used in practice

$$\int n_e \, dl = 4.97 \times 10^{14} \sin^{-1} \left(\frac{I}{I_o}\right)$$

We must consider the effects of neutral atoms and ions on the interferometer measurement. Recalling

$$(n-1)_e = 1.77 \times 10^{-22} n_e$$

we compare[65]

$$(n-1)_{H_2} = 4.7 \times 10^{-24} N_{H_2}$$

$$(n-1)_{He} = 9.6 \times 10^{-25} n_{He}$$

$$(n-1)_{H^+} = \left(\frac{m_e}{m_H}\right) (n-1)_e \approx 0$$

Contributions from H and $He^+$ are similarly small. Excited states may have coefficients an order of magnitude or two larger than those of the ground state of the corresponding atom, but populations of excited states are usually very low. One must avoid using wavelengths for the interferometer which are very close to an atomic transition. Otherwise the resonant effect might be overwhelming. We can see that the largest contribution will come from hydrogen but for a plasma with significant ionization it can be neglected.

Next we consider the effect of spatial gradients on the

beam propagation. The angle of deflection for a beam passing through a medium with a perpendicular gradient in the index if refraction n, is

$$\theta = \int \frac{\nabla n}{n} \, d\ell$$

if $n = 1 - \alpha n_e$

$$\nabla n = -\alpha \nabla n_e$$

$$\theta = -\alpha \int \nabla n_e \, dl \qquad (\alpha n_e << 1)$$

$$= 1.77 \times 10^{-22} \int \nabla n_e \, dl$$

for a uniform density along a path length L.

$$\theta = 1.77 \times 10^{-22} \, n_e \frac{L}{L_n} \qquad L_n = \text{density scale length}$$

This effect will be significant when $\theta$ approaches the divergence of the laser used in the interferometer. In the present experiment the larges $n_e L$ encountered is $10^{17}$, the beam divergence is about $10^{-3}$ radians. So we require, to ignore the effect

$$10^{-3} >> 1.77 \times 10^{-5}/L_n$$

or

$$L_n >> .02 \text{ cm}$$

This is much smaller than an ion gyroradius for any reasonable set of parameters in the present experiment.

Another possible problem is Faraday rotation in the glass vacuum windows. The effect would be to rotate the angle of polarization of one beam and change the interference pattern.

For soda-lime glass

$$\theta_{FR} = 2 \times 10^{-6} \text{ B(kG) L(cm)}$$

for quantity

$$\theta_{FR} = 4.6 \times 10^{-7} \text{ BL}$$

In the present experiment L = 2.5 cm

$$\theta_{FR} = 5 \times 10^{-6} \text{ B (kG)}$$

$$\theta_{FR}/\theta_{n_e} < 3 \times 10^{-5} \text{ B (kG)} << 1$$

Figure 33 shows the physical arrangment for the interferometer used on TORMAC IV-c. It was built by B. Feinberg. The feedback stabilization circuit was designed by B. Myers.

In order to overcome the problem of mechanical vibrations and acoustic oscillations and thermal drifts that plague sensitive interferometers, a feedback stabilization network has been incorporated into the system. Such a scheme is useful when the unwanted vibrations are on a time scale slower than that characteristic of the plasma. For Tormac we are interested in times no longer than 100 microseconds. Vibrations are typically in the range of a few kHz and below. The circuit is then set to hold the fringe pattern constant. It responds and adjusts for extraneous vibration, but is unable to follow the rapid variations that accompany a plasma shot. The system is closed loop for slow changes and open loop for fast ones.

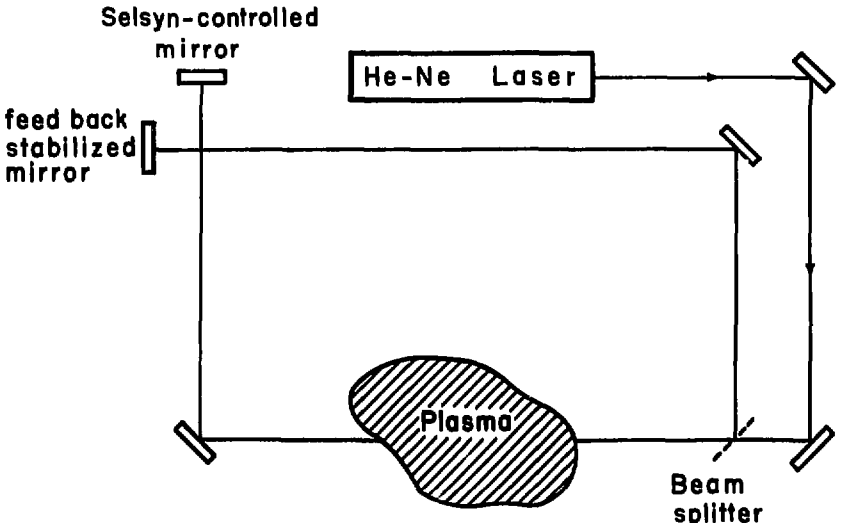


He-Ne Interferometer

XBL 789-2207

Fig. 33

A portion of the output signal is amplified and frequency compensated. It is then fed to a speaker cone which drives the reference arm mirror. Stabilization to 1/1000 of a fringe was obtained with very careful adjustment of the current; 1/100 fringe is available routinely for a sensitivity of 5 x $10^{14}/cm^2$ over a 10 cm path. This would correspond to an average density of 5 x $10^{13}/cm^3$. Typical TORMAC density are two orders of magnitude higher.

To aid in alignment, a pair of selsyns drive the plasma arm mirror. The interferometer is self-contained and can be moved up and down on pulleys to scan across the plasma.

Magnetic Probes

A crucial measurement of a plasma is the determination of internal fields and currents. While nonperturbing methods have been developed; they tend to be elaborate and expensive and are often limited in the range of plasma parameters they apply to. In the absence of a more palatable alternative, magnetic probes can be used. They almost certainly perturb the plasma as they are placed in its midst. Under certain conditions this perturbation can be small and reliable measurements can be made.

The magnetic probes used on TORMAC IV consist of two small rectangles .25 x .7 cm of 15 turns of #38 wire, enclosed in a quartz tube .4 cm in diameter. The two coils measure the two components of the magnetic field. The wires are

twisted back through the probe and joined to coaxial cable. A third cable is connected to a dummy probe. It consists only of a twisted wire and measures the level of electrostatic pickup. In the experiment, pickup levels were small and additional shielding was not necessary.

The response of the coil to changing magnetic fields is

$$V = \frac{nA}{c}\frac{\partial B}{\partial t}$$

n = number of turns
A = coil area in $cm^2$
B is measured in Gauss
V is measured in statvolts

The coils have an nA = 1.73 $cm^2$. They are used with an RC integrator of time constant 100 microseconds. Response is

$$V_{(volts)} \simeq \frac{10^{-8}nAB}{\tau_{RC}} = 1.73 \times 10^{-4}B$$

The coil inductance is about 2 μH. With a 50 Ω load frequency response of the probes should be good to almost 10 MHz. By comparison, the cusp rise time is 8.3 microseconds, an Alven wave will traverse the plasma in about 1 microsecond.

We would like to show that perturbations, caused by introduction of the probe into the plasma, are not serious. Lovberg calculates the boil off time of probe material by considering the transient response of various materials (glass, quartz, alumina) to heat loads at their surface; heat in this case, coming from the plasma.[66] He obtains the result for

quartz

$$t_b = \frac{5.1 \times 10^{29}}{n^2 T^3 (eV)}$$

F typical TORMAC IV parameters, $T_e \sim 5$ eV, $n_e \sim 5 \times 10^{15}$, $t_b \approx 150$ microseconds, which is tolerable.

Spectroscopic Hardware

For measuring spectral profiles, a 3/4 meter Czerny-Turner spectrometer was used. A cylindrical lens focuses the exit slit onto an array of 16 plastic light guides, each approximately 11 mm wide. The light guides direct the light to 16 RCA 4840 photomultipliers. The instrumental dispersion is 11A/mm; the lens magnifies the image by 3. Thus each channel is 11/3 x .11 = .4 A wide. Sixteen operational amplifiers (National 531) and emitter followers are mounted in the polychromator housing near the photo multipliers. Gains are adjustable from $10^4$ to $10^6$ V/A. Frequency response is better than 1 MHz. The 4840's have a fairly broad spectral response. The polychromator input is coupled to a light pipe made of 10 mil fibers. The individual fibers are aligned at one end to match the slit shape. A lens and mirror arrangement (see Figure 34) attached to the other end serves to gather light from a narrow cone and focus it onto the light pipe. With this arrangement one can scan, without tedious alignment, various regions of the plasma with good spatial resolution. A good deal of light is lost, due to insertion losses and attentuation in the fiber optics. However, the

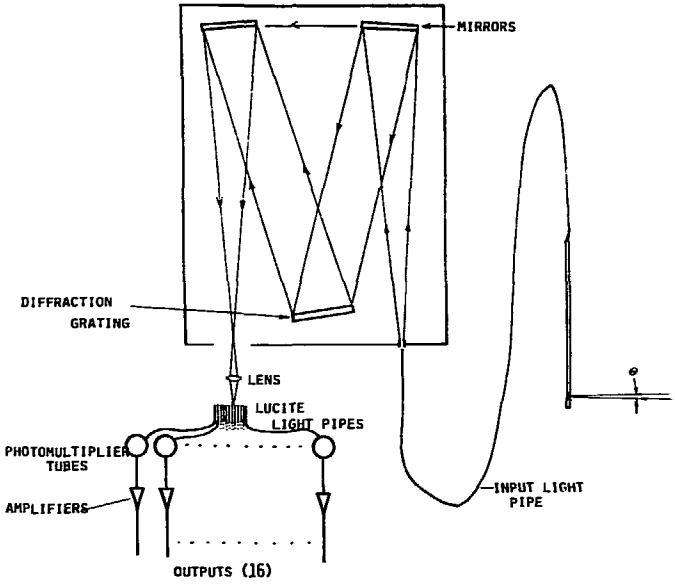


SIXTEEN CHANNEL POLYCHROMATOR AND LIGHT PROBE. SEPARATION BETWEEN CHANNELS IS .39 A.

XBL 789-10876

Fig. 34

plasma is quite bright at the wavelengths of interest.

Rogowski Coils and Flux Loops

Rogowski coils are used to measure the current flowing in the cusp windings, the preionize and bias coils; to monitor the firing of the ignitrons and to measure current flowing in the plasma.

The belt measuring plasma current was wound as uniformly as possible, 20 turns per cm, backwound. Considerations of sensitivity, calibration and response time are similar to those for magnetic probes. The coil inductance was 8 μH. With a 50 Ω load its response time was .15 microseconds. The belt was insulated with PVC tubing.

A diamagnetic loop was used to measure integrated toroidal flux. The loop was a single turn of insulated wire wrapped around the vacuum vessel. With a suitable voltage divider and integrator the response of the loop

$$\int E \cdot d_s = \frac{1}{c} \frac{\partial}{\partial t} \int B \cdot dA$$

$$V_{volts} = -9.2 \times 10^{-7} \int B \cdot dA$$

for toroidal flux $B \sim I_o/5R$ .

So $V = 1.8 \times 10^{-7} W I_o \ell n \left(\frac{R_{max}}{R_{min}}\right)$

$W$ = width of vessel

$R_{max}$ = outer radius

$R_{min}$ = inner radius

REFERENCES

1. Furth, H. P., Adv. in Plasma Physics, Vol. 1, Simon, A., and Thompson, W. B., eds., John Wiley, N. Y. (1968) p. 67.

2. Braginskii, S. I., and Kadonstev, B. B., Plasma Physics and the Problems of Controlled Thermonuclear Reactions, Vol. 3, Pergamon Press (1959), p. 356.

3. Berkowitz, J., Grad, H., and Rubin H., Proc. 2nd U.N. Conf. on Peaceful Uses of Atomic Energy, Vol. 31, United Nations, Geneva, (1958), p. 177.

4. Spalding, I. J., Adv. in Plasma Phys., Vol. 4, Simon and Thomson, eds., Interscience (1971). p. 79.

5. Berkowitz, J., loc. cit., p. 177.

6. Berkowitz, J., Frederichs, K. O., Goertzel, H., Grad, H., Killeen, J., and Rubin, E., Proc. 2nd U. N. Conf. on Peaceful Uses of Atomic Energy, Vol 31, United Nations, Geneva (1958), p. 171.

7. Grad, H., and Rubin H., Proc. 2nd U. N. Conf. on Peaceful Uses of Atomic Energy, Vol. 31, United Nations, Geneva (1958) p. 190.

8. Levine, M. A., Boozer, A. H., Kalman, G., and Bakshi, P., Phys. Rev. Lett. 20, 1323 (1972).

9. Boozer, A. H., and Levine, M. A., Phys. Rev. Lett., 31, 1287 (1973).

10. Combes, L. S., Gallagher, C. C., and Levine, M. A., Phys. Fluids, 5, 1070 (1962).

11. Allen, T. K., et al., Phys. Fluids, 9, 1394 (1966).

12. Belitz, H. J., and Kugler, E., Plasma Physics and Controlled Nuclear Fusion Research, Vol. 1, IAEA, Vienna (1966) p. 298.

13. Spalding, I. J., et. al., Plasma Physics and Controlled Nuclear Fusion Research, Vol. 2, IAEA, Vienna, (1969) p. 639.

14. Junker, J., and Lotz, W. Z., Physik, 238, 148, (1970).

15. Shimonura, Y., et. al., Nucl. Fusion, 16, 587 (1976).

16. Grad, H., Phys. Fluids, 9, 2472 (1966).

17. Hamasaki, S., Davidson, R. C., Krall, N. A., Liewer, P. C., Nuclear Fusion, 14, p. 27 (1975).

18. Coensgen, F. H., et. al., Phys. Rev. Lett., 35, 1501 (1975).

19. Zelenzi, L. M., Sov. J. Plasma Phys. 1, 319 (1975).

20. Gladd, N. T., et. al., (Internal report) Tormac Theory Workshop, LBL, (1976).

21. Baldwin, D. E., Berk, H. L., and Pearlstein, L. D., Phys. Rev. Lett., 36 1051 (1976).

22. Krall, N. A., Phys. Fluids, 20, 311 (1977).

23. Levine, M. A., Bul. Am. Phys. Soc., 17, 1040 (1972).

24. Ibid.

25. Gallagher, C. C., Combes, L. S., and Levine, M.A., Phys. Fluids, 13, 1617 (1970).

26. Gallagher, C. C., and Levine, M. A., AFCRL Physical Sciences Research Paper # 590 AFCRL-TR-74-0122, (1974).

27. Levine, M. A., Boozer, A., Kunkel, W., Proc. of the High Beta Workshop, Los Alamos 1975, ERDA-76/108.

28. Levine, M. A., Brown, I. G., and Gallagher, C.C., Lawrence Berkeley Lab. Report LBL-3262 (1975).

29. Salpeter, E. E., Phys. Rev., 120, 1528 (1960).

30. Salpeter, E. E., Phys. Rev., 122, 1663 (1961).

31. Book, D. L., NRL Memorandum #3332.

32. Seaton, M. J., Planet Space Sci., 12, 55 (1964).

33. McWhirter, R. W. P., Plasma Diagnostic Techniques, Chap. 5, Huddleston and Leonard eds., Academic Press, N. Y., (1965) p. 221.

34. Freeman, R. L., Jones, E. M., UKAEA Report, Atomic Collision Processes in Plasma Physics Experiments, Culham Laboratory (1974).

35. Spitzer, L., Physics of Fully Ionized Gases 2nd ed., John Wiley, N. Y. (1962) p. 144.

36. Griem, H., Spectral Line Broadening by Plasmas, Academic Press, N. Y. (1974) p. 220.

37. Dreicer, H., Phys. Rev., 115, 238 (1959).

38. Rose, D. J., and Clark, M., Plasma and Controlled Fusion, M.I.T. Press (1961) p. 175.

39. Combes, L. S., Gallagher, C. C., amd Levine, M.A., Rev. Sci. Instr., 37, 1567 (1966).

40. Weast, R. C., ed., Handbook of Tables for Applied Engineering Science, CRC Press, Cleveland (1973) p. 149.

41. Roark, R. J., and Young, W. C., Formulas for Stress and Strain, 5th ed., McGraw Hill N. Y., p. 338.

42. Holland, L., Steckelmacher, W., and Yarwood, J., Vacuum Manual, E. and F. N. Spon, London (1974).

43. Coonrod, J. W., Digitizing High Frequency Signals Using Serial Analog Memories, LBL-4468 (1975).

44. Fiocco, G., and Thompson, E., Bull. Am. Phys. Soc., 8, 372 (1963).

45. Ramsden, S. A., and Davies, W. E. R., Phys. Rev. Lett., 13, 227 (1964).

46. Peacock, N. J., Robinson, D. C., Forrest, M. J., Wilcock, P. D., and Sannikov, V. V., Nature 224, 488 (1968).

47. Evans, D. E., and Katzenstein, J., Rep. Prog. Phys., 32, 207 (1969).

48. Ramsden, S. A., Physics of Hot Plasmas, Rye and Taylor, eds., Scottish Universities Summer School 1968, Oliver and Boyd, Edinburgh (1970).

49. DeSilva, A. W., and Goldenbaum, G. C., Plasma Diagnostics by Light Scattering, Part III of Methods of Experimental Physics Vol. IX, Part A, Academic Press, N. Y., (1970).

50. Rosenbluth, M. N., and Rostoker, N., Phys. Fluids, 5, 776 (1962).

51. Bekefi, G., Radiation Processes in Plasmas, John Wiley, N. Y., (1966).

52. Kunze, H. J., Plasma Diagnostics, Chap. 9, W. Lochte-Holtgreven, ed., North Holland, Amsterdam (1968).

53. Sheffield, J., Plasma Scattering of Electromagnetic Radiation, Academic Press, N. Y., (1975).

54. Dougherty, J. P., and Farley, D. T., Proc. Roy. Soc., A259, 79 (1960).

55. Buneman, O., J. Geophys. Res., 67, 2050 (1962).

56. Spitzer, L., op. cit., p. 148.

57. Kunze, H. J., op. cit., p. 589.

58. Cullom, H. J., and Waynant, R. W., Appl. Opt., 3, 989 (1964).

59. Yamanaka, C., et. al., Conference on Damage of Laser Materials, Boulder 1971, IQEC 20-3 p. 404.

60. Yamanaka, C., Laser Interaction and Related Plasma Physics Phenomenon Vol. 2, Schwarz and Hora, eds., Plenum Press, N. Y., (1972) p. 481.

61. Siemon, R. E., Appl. Opt., 13, 699 (1974).

62. VanCittert, P. H., Z. Instr., 46, 557. (1926).

63. Greenwald, M., and Smith, W. I. B., Appl. Optics, 16, 587 (1977).

64. Glasstone, S. amd Lovberg, R. H., Controlled Thermonuclear Reactions, Van Nostrand-Reinhold, Princeton (1960).

65. Gray, D. E., ed., American Institute of Physics Handbook 3rd edition, McGraw Hill, N. Y. (1972).

66. Lovberg, R. H., Plasma Diagnostics Techniques Chap. 3, Huddlestone and Leonard eds., Academic Press, N. Y., (1965) p. 105.

67. Burch, G., Introduction to Matrix Methods in Optics, John Wiley, N.Y. (1975).